Discreteness effects on the double sine-Gordon kink

P. Tchofo Dinda
Laboratoire de Physique, Université de Bourgogne, 6 Boulevard Gabriel, 21000 Dijon, France

C. R. Willis
Department of Physics, Boston University, 590 Commonwealth Avenue, Boston, Massachusetts 02215
(Received 7 November 1994)

We derive and analyze the exact collective variable equations of motion for the discrete double sine-Gordon (DSG) equation as a typical example of a discrete Klein-Gordon equation with an internal mode. In the continuum DSG system, the small-amplitude equations of motion for the center of mass $X(t)$ and internal mode $R(t)$ are uncoupled, but discreteness causes the center of mass mode $X(t)$ and the internal mode $R(t)$ to be strongly coupled, leading to further qualitative phenomena in addition to the known discreteness phenomena such as the Peierls-Nabarro potential and effects due to internal modes. We show that the behavior of large kinks where the distance between subkinks is large compared to the size of the subkink is different from the behavior of small kinks where the distance between subkinks is smaller than the size of the subkink. In the case of the small kink, we show that there are two minima per unit cell instead of the usual one minimum and that the discrete DSG kink becomes temporarily trapped and untrapped due to conversion of center of mass energy to internal mode energy and back until the kink finally becomes permanently trapped. We show by simulations that the radiation occurs in bursts and decreases sharply at specific frequencies, which can be straightforwardly explained by collective variable theory. In addition, the asymmetry of the phonon radiation by the moving DSG kink is responsible for asymmetries in the subkink-subkink interaction, causing phenomena such as excitation of the internal mode and causing the subkinks to travel sometimes at different speeds. We determine the exact Peierls-Nabarro and internal mode small oscillation frequencies.

PACS number(s): 03.40.Kf

I. INTRODUCTION

There are several problems in nonlinear Klein-Gordon and similar systems which are difficult to understand in terms of the original field variables $\phi(x,t)$ [or $\phi(n,t)$ in the discrete version] that can be readily understood using a collective variable (CV) approach. For example, in a discrete lattice the familiar problem of the Peierls-Nabarro (PN) potential can be treated as a "point" particle $X(t)$, which satisfies an ordinary differential equation, moving in a nonlinear periodic potential where the period of the potential is the period of the lattice. The radiation from the kink caused by the discreteness can usually be treated as a linear radiation field driven by the acceleration of the point particle $X(t)$, which is determined by the nonlinear periodic force on $X(t)$. The rich spectrum of radiation by trapped and untrapped kink motion which expresses the phonon radiation generated by the nonlinear motion of the center of mass $X(t)$ can be straightforwardly understood by the CV approach. Another situation where a CV approach gives useful insight into the behavior of a nonlinear field equation is that of an internal mode of a kink such as the double sine-Gordon (DSG) kink [1], where the distance between the subkinks—which is proportional to the parameter $\Re$ which appears in the DSG potential energy [2]—is represented by a collective variable $R(t)$. The time variation in $R(t)$ is caused by some perturbation applied to the DSG kink which causes the distance between the subkinks to vary, e.g., when two DSG kinks collide [3,4].

One of the main results of this paper is to show that discretizing the continuum DSG equation generally causes the separation between subkinks to become time dependent so that we have $R(t)=\Re+Y(t)$, where $Y(t)$ describes the time variation of $R(t)$ about $\Re$. Furthermore, the discreteness causes $X(t)$ and $R(t)$ to be strongly coupled. We find that the resultant strong coupling between the center of mass (c.m.) $X(t)$ and the internal mode $R(t)$ leads to qualitatively different phenomena such as temporary trapping and untrapping of the kink. Some of these phenomena are a consequence of the interaction between X and R causing two potential minima in a cell in those cases where the distance between the subkinks is less than the size of a subkink. We also find different qualitative behavior when the phonons radiated by one subkink interact with the other subkink introducing asymmetries in the moving DSG kink as a consequence of the asymmetry of the radiation in the forward and backward directions of a moving kink. We also analyze the properties of the radiation leaving the kink in both the trapped and untrapped cases.

In Sec. II we briefly review the properties and solutions of the DSG equation. Then we give the exact equations of motion of the DSG system in terms of the collective variables. We take as initial conditions the exact static solution of the discrete DSG equation obtained by the classical pseudodynamics relaxation process. In Sec. III we present the derivation of the equations of motion for the c.m. $X(t)$ and the expression of its frequency of oscil-

lation in the weakly discrete limit, for the case of constant separation between the subkinks, $R(t)=\Re$. We also derive the equations of motion for the internal mode $R(t)$, and obtain the lowest-order expression for its frequency of oscillation by keeping the c.m. fixed at a minimum of the PN potential. The frequencies corresponding to these two modes lie in the gap below the phonon band. Also we perform the exact determination of the frequencies of the two modes by numerically finding the eigenvalues of small oscillations about the exact discrete kink ground state. The exact numerical and calculated frequencies agree very well for $\Re<\Re_c$, where $\Re_c$ is as yet an unknown quantity whose value depends only upon the importance of the discreteness. The reason for the deviations for $\Re>\Re_c$ are explained. In Sec. IV we present and analyze the simulations of the CV equations of motion. We first consider DSG kinks where the distance between the subkinks is large compared with the size of each subkink. The first simulation considers the excitation of the internal mode keeping the c.m. fixed at a minimum of the PN potential. When the internal mode is excited nonlinearly, it radiates mainly in bursts as harmonics of the internal mode frequency enters the phonon band. Next, we start with the internal mode initially unexcited but with X not at a minimum of the PN potential. Since the symmetry is broken, the internal mode becomes excited and there is a regular exchange of energy between the center of mass mode and the internal mode. We consider next the untrapped case with the same initial conditions as above except with a higher initial velocity so that the DSG kink is no longer trapped initially. When we start with the internal mode unexcited initially it becomes excited. When the untrapped kink moves, it radiates phonons and its frequency decreases. When the frequency crosses the lower phonon band edge and goes into the band gap there is a sharp decrease in the rate of radiation. Finally, we repeat the above cases for a kink in which the intersubkink spacing is equal to or less than the size of the subkinks so that the subkinks have essentially lost their individual identities. For the case of subkinks that are very close to each other we find completely different qualitative behavior which arises from the fact that there are now two minima in a unit cell instead of just the usual simple PN minimum. Finally in Sec. V we conclude.

II. COLLECTIVE VARIABLE THEORY

The Lagrangian for the DSG system is written

$$\bar{L}=\frac{m}{2}\sum_n\left[\frac{du_n}{d\tau}\right]^2-\tfrac{1}{2}\mu\sum_n(u_{n+1}-u_n)^2-\frac{W}{2}\sum_n V_{\mathrm{DSG}}(4\pi u_n/a)\ , \tag{2.1}$$

where u_n is the position of the nth particle of mass m measured from the nth lattice site, μ is the effective spring constant between adjacent particles, τ is the time, a is the period of the substrate potential V_{DSG}, and W serves as a measure of its amplitude. The expression of V_{DSG} will be given explicitly below. When the dimensionless variables are introduced in Eq. (2.1) the Lagrangian becomes

$$L\equiv\frac{(4\pi)^2}{\mu a^2}\bar{L}=\tfrac{1}{2}\sum_n\left[\frac{dQ_n}{dt}\right]^2-\tfrac{1}{2}\sum_n(Q_{n+1}-Q_n)^2-\left[\frac{2\pi}{L_0}\right]^2\sum_n V_{\mathrm{DSG}}(Q_n)\ , \tag{2.2}$$

where $Q_n\equiv 4\pi u_n/a$, $t\equiv(\sqrt{\mu/m}\,)\tau$ is the dimensionless time, $L_0\equiv\sqrt{\mu a^2/2W}$ is the dimensionless coupling constant that serves as a measure of the importance of the force between the particles relative to the force due to the substrate potential, and hence L_0 can serve as a measure of the importance of discreteness effects.

The substrate potential of the DSG model is doubly periodic:

$$V_{\mathrm{DSG}}(\phi)=\frac{4}{1+4|\eta|}\left[\left[1-\cos\frac{\phi}{2}\right]+\eta(1-\cos\phi)\right]\ , \tag{2.3}$$

where $-\infty\le\eta\le+\infty$ is an arbitrary parameter. When $\eta=0$ one obtains a SG potential where $-2\pi\le\phi\le 2\pi$ (modulo 4π), and when $\eta=\pm\infty$, Eq. (2.3) becomes a SG potential where $-\pi\le\phi\le\pi$ (modulo 2π). Otherwise the potential (2.3) exhibits a variety of structures depending on the value of η (see Ref. [2]). For instance, for $\frac{1}{4}<\eta<+\infty$, the potential possesses two nondegenerate minima, and admits only one type of kink solution. In this region of η, the potential (2.3) can be rewritten in terms of a new parameter $\Re$ defined by

$$\eta\equiv\tfrac{1}{4}\sinh^2\Re\ . \tag{2.4}$$

The physical meaning of $\Re$ will be clarified later on. In terms of $\Re$, the potential reads

$$V_{\mathrm{DSG}}(\phi)=V_{\Re}(\phi)\equiv\frac{4}{\cosh^2\Re}\left[1+\cos\left[\frac{\phi}{2}\right]\right]+(1-\cos\phi)\tanh^2\Re\ . \tag{2.5}$$

Figures 1(a) and 1(b) show the shape of $V_{\Re}(\phi)$ for different values of $\Re$.

In the present paper we examine discreteness effects on a DSG system described by the potential (2.5). The discrete equation of motion is then given by

$$\ddot{Q}_n-\Delta_2 Q_n+\omega_0^2\frac{dV_{\Re}}{dQ_n}(Q_n)=0\ , \tag{2.6}$$

where the second difference Δ_2 is defined as $\Delta_2 h_n\equiv h_{n-1}+h_{n+1}-2h_n$, an overdot indicates differentiation with respect to the time t, and

$$\omega_0\equiv 2\pi/L_0\ . \tag{2.7}$$

For setting up a collective variable treatment of the dynamics we decompose the field Q_n in the following way:

$$Q_n=f_n+q_n\ , \tag{2.8}$$

where f_n is a suitably chosen ansatz function of the col-

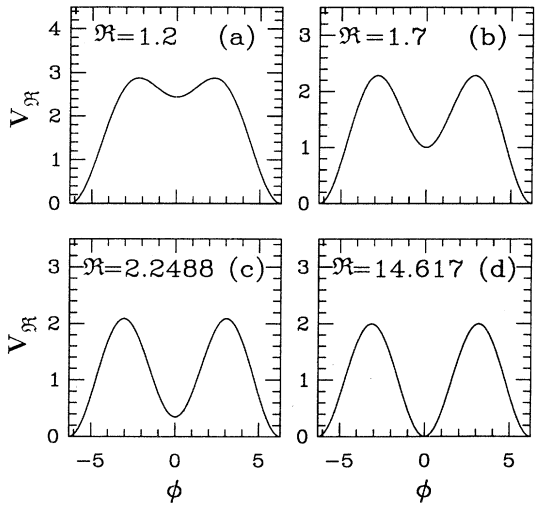

FIG. 1. Plot of the DSG potential $V_\Re$, Eq. (2.5), for $\Re=$ (a) 1.2; (b) 1.7; (c) 2.2488; (d) 14.617.

lective coordinates, and q_n is then the remaining field such that the sum of f_n and q_n satisfies Eq. (2.8). Before going through the derivation of the equations of motion for the collective variables, it is desirable to first address the problem of choosing an ansatz function that provides a best representation of the configuration of the discrete DSG kink. In this respect we recall that in the continuum limit the static kink solution for the DSG system is [1]

$$\sigma(x,X,\Re)=\sigma_{\rm SG}[\omega_0(x-X)+\Re] -\sigma_{\rm SG}[-\omega_0(x-X)+\Re] , \tag{2.9}$$

where

$$\sigma_{\rm SG}[\phi]\equiv 4\tan^{-1}[\exp(\phi)] ,$$

x is a continuous position variable, and X a collective coordinate that locates the c.m. of the DSG kink. Equation (2.9) expresses the fact that the static kink solution for the DSG system can be rigorously expressed in terms of the single kink solutions of the SG system. Furthermore, Eq. (2.9) can be rewritten in such a way that the parameters ω_0 and $\Re$ are given their physical meaning, in the following way:

$$\sigma(x,X,\Re)=\sigma(x,X_1,X_2) =\sigma_{\rm SG}[\omega_0(x-X_1)]-\sigma_{\rm SG}[-\omega_0(x-X_2)] , \tag{2.10}$$

where $X_1=X-\Re/\omega_0$ and $X_2=X+\Re/\omega_0$ locate the c.m. of the two subkinks. Equation (2.10) shows that in the continuum limit the slope of each subkink is ω_0, and the distance that separates the subkinks is

$$\mathcal{D}_0=X_2-X_1=2\Re/\omega_0 . \tag{2.11}$$

Therefore the parameter $\Re$ determines the separation between the two subkinks (in units of $2/\omega_0$).

So, for setting up the CV treatment, we choose the ansatz function to be the continuum solution for the DSG kink, evaluated at discrete lattice points. That is, we consider the following ansatz function:

$$f_n[X(t),Y(t),Z]=\sigma_{\rm SG}[Z\{\omega_0(n-X)+\Re+Y\}] -\sigma_{\rm SG}[Z\{-\omega_0(n-X)+\Re+Y\}] , \tag{2.12}$$

where we have replaced the continuous position variable x by the site index n, and introduced another collective variable $Y(t)$ and a parameter Z. The collective coordinate Y describes the variation of the distance between the subkinks due to any perturbation that changes the distance from the value of $\Re$ in Eq. (2.10) such as radiation, discreteness, or kink-kink collisions. The parameter Z is as yet an unknown quantity whose value will be chosen depending on the importance of discreteness effects. Note that Eq. (2.12) is expressed in such a way that only collective variables which describe the DSG kink as a whole collective entity appear explicitly, that is, X and Y. However, this ansatz can also be rewritten in such a way that there appear explicitly collective variables which describe the DSG kink as two bound collective entities (which are the subkinks), in the following way:

$$f_n(X,Y,Z)=f_n(X_1,X_2,Z) =\sigma_{\rm SG}[\omega_0 Z(n-X_1)]-\sigma_{\rm SG}[-\omega_0 Z(n-X_2)] , \tag{2.13}$$

where

$$X_1=X-(\Re+Y)/\omega_0 \tag{2.14a}$$

and

$$X_2=X+(\Re+Y)/\omega_0 \tag{2.14b}$$

represent, respectively, the centers of the two subkinks which make up the DSG kink. The distance between the two subkinks is then

$$\mathcal{D}\equiv X_2-X_1=2(\Re+Y)/\omega_0 , \tag{2.14c}$$

and the slope of each of the subkink is

$$\xi\equiv\omega_0 Z . \tag{2.14d}$$

The CV approach that we use in the present paper is the projection-operator approach [5], which was shown to make the derivation of the CV equations of motion extremely simple. According to this approach one needs to specify four constraints which give the collective variables X and Y their physical meaning, and they are

$$C_{1X}=\langle f_{n,X}|q_n\rangle=0, \quad C_{2X}=\langle f_{n,X}|p_n\rangle=0 , \tag{2.15}$$

where the bracket notation means sum over the particle

index and p_n is the momentum conjugate to q_n. In these expressions an index after a comma stands for partial differentiation with respect to the collective coordinate denoted by the index. The constraint conditions for Y, C_{1Y}, and C_{2Y} are obtained from the expressions of C_{1X} and C_{2X}, respectively, in Eq. (2.15), by replacing $f_{n,X}$ by $f_{n,Y}$. Substituting Eqs. (2.8) and (2.12) into the equation of motion (2.6) yields

$$\ddot{q}_n+\ddot{X}f_{n,X}+\dot{X}^2f_{n,XX}+\ddot{Y}f_{n,Y}+\dot{Y}^2f_{n,YY} -(\Delta_2 f_n+\Delta_2 q_n)+2\dot{X}\dot{Y}f_{n,XY} +\omega_0^2\frac{dV_{\Re}}{dQ_n}[Q_n=f_n+q_n]=0 . \quad (2.16)$$

Projecting Eq. (2.16) in the directions $\langle f_{n,X}|$ and $\langle f_{n,Y}|$, respectively, yields

$$\langle f_{n,X}|\ddot{q}_n\rangle+\ddot{X}M_X+\dot{X}^2\langle f_{n,X}|f_{n,XX}\rangle+\ddot{Y}M_{XY}+\dot{Y}^2\langle f_{n,X}|f_{n,YY}\rangle+2\dot{X}\dot{Y}\langle f_{n,X}|f_{n,XY}\rangle -(\langle f_{n,X}|\Delta_2 f_n\rangle+\langle f_{n,X}|\Delta_2 q_n\rangle)+\omega_0^2\left\langle f_{n,X}\left|\frac{dV_{\Re}}{dQ_n}[Q_n=f_n+q_n]\right.\right\rangle=0 , \quad (2.17)$$

$$\langle f_{n,Y}|\ddot{q}_n\rangle+\ddot{Y}M_Y+\dot{Y}^2\langle f_{n,Y}|f_{n,YY}\rangle+\ddot{X}M_{XY}+\dot{X}^2\langle f_{n,Y}|f_{n,XX}\rangle+2\dot{X}\dot{Y}\langle f_{n,Y}|f_{n,XY}\rangle -(\langle f_{n,Y}|\Delta_2 f_n\rangle+\langle f_{n,Y}|\Delta_2 q_n\rangle)+\omega_0^2\left\langle f_{n,Y}\left|\frac{dV_{\Re}}{dQ_n}[Q_n=f_n+q_n]\right.\right\rangle=0 , \quad (2.18)$$

where

$$M_X=\langle f_{n,X}|f_{n,X}\rangle,\quad M_Y=\langle f_{n,Y}|f_{n,Y}\rangle ,\quad M_{XY}=\langle f_{n,X}|f_{n,Y}\rangle . \quad (2.19)$$

The terms $\langle f_{n,X}|\ddot{q}_n\rangle$ in Eq. (2.17) and $\langle f_{n,Y}|\ddot{q}_n\rangle$ in Eq. (2.18) are replaced by taking, respectively, the second time derivative for C_{1X} and C_{1Y}, and substituting the resultant equation into (2.17) and (2.18): we obtain

$$A_1\ddot{X}+B\ddot{Y}=K_1 , \quad (2.20)$$

$$B\ddot{X}+A_2\ddot{Y}=K_2 , \quad (2.21)$$

where

$$A_1=M_X-\langle f_{n,XX}|q_n\rangle , \quad (2.22)$$

$$B=M_{XY}-\langle f_{n,XY}|q_n\rangle , \quad (2.23)$$

$$A_2=M_Y-\langle f_{n,YY}|q_n\rangle , \quad (2.24)$$

$$K_1=\dot{X}^2(\langle f_{n,XXX}|q_n\rangle-\langle f_{n,X}|f_{n,XX}\rangle)+\dot{Y}^2(\langle f_{n,XYY}|q_n\rangle-\langle f_{n,X}|f_{n,YY}\rangle) +2\dot{X}\langle f_{n,XX}|\dot{q}_n\rangle+2\dot{Y}\langle f_{n,XY}|\dot{q}_n\rangle+2\dot{X}\dot{Y}(\langle f_{n,XXY}|q_n\rangle-\langle f_{n,X}|f_{n,XY}\rangle) +(\langle f_{n,X}|\Delta_2 f_n\rangle+\langle f_{n,X}|\Delta_2 q_n\rangle)-\omega_0^2\left\langle f_{n,X}\left|\frac{dV_{\Re}}{dQ_n}[Q_n=f_n+q_n]\right.\right\rangle . \quad (2.25)$$

K_2 has the same expression as K_1, but with X and Y interchanged, as also $\partial/\partial X$ and $\partial/\partial Y$. Solving Eqs. (2.20) and (2.21) for $\ddot{X}$ and $\ddot{Y}$ we obtain

$$\ddot{X}=(K_1A_2-K_2B)/(A_1A_2-B^2) , \quad (2.26)$$

$$\ddot{Y}=(K_2A_1-K_1B)/(A_1A_2-B^2) . \quad (2.27)$$

Then solving Eq. (2.16) for $\ddot{q}_n$ we obtain

$$\ddot{q}_n=-\left[\ddot{X}f_{n,X}+\dot{X}^2f_{n,XX}+\ddot{Y}f_{n,Y}+\dot{Y}^2f_{n,YY} -(\Delta_2 f_n+\Delta_2 q_n)+2\dot{X}\dot{Y}f_{n,XY} +\omega_0^2\frac{dV_{\Re}}{dQ_n}[Q_n=f_n+q_n]\right] , \quad (2.28)$$

where the values of $\ddot{X}$ and $\ddot{Y}$ obtained from Eqs. (2.26) and (2.27) are to be substituted into the right-hand side of Eq. (2.28). Thus, the set of equations (2.26), (2.27), and (2.28) determine the time evolution of X, Y, and q_n, starting from some specified initial conditions, whether the kink is trapped or untrapped.

For suitably solving the CV equations of motion (2.26), (2.27), and (2.28), extreme care must be taken in choosing the initial conditions for the system. In particular, those initial conditions must be chosen in such a way that the constraint conditions (2.15) are satisfied at time $t=0$. To this end, our initial kink profile $Q_n(t=0)$ will always consist of the exact kink solution of the discrete DSG system, obtained via the classical pseudodynamics relaxation process. Then we obtain the initial conditions for the collective variables by determining the values

$X(t=0), Y(t=0)$, and Z, for which $f_n(X,Y,Z)$ is the best fit to the initial kink profile $Q_n(t=0)$, by minimizing

$$\Lambda \equiv \sum_n q_n^2(0) = \sum_n [Q_n(0) - f_n(X,Y,Z)]^2 . \tag{2.29}$$

The minimum of Λ with respect to X and Y yields $\partial\Lambda/\partial X = 0$ and $\partial\Lambda/\partial Y = 0$, which correspond in fact to the first constraint conditions $C_{1X}=0$ and $C_{1Y}=0$, respectively. Note also that the minimum of Λ with respect to Z corresponds in fact to the first constraint condition for Z if we were to treat Z as a collective variable. However, in the present paper we do not treat Z as a collective variable, but rather as a constant whose value we obtain from Eq. (2.29). Furthermore, the initial velocities of the particles will be chosen to be of the form

$$\dot{Q}_n(0) = \frac{\epsilon_X}{\Delta t} f_{n,X} + \frac{\epsilon_Y}{\Delta t} f_{n,Y} , \tag{2.30}$$

where Δt is the molecular dynamics time step and ϵ_X and ϵ_Y are small parameters. This expression (for the initial velocities of the particles) leads to the initial conditions for the velocities for the CV, $\dot{X}(0)$ and $\dot{Y}(0)$, for which the second constraint conditions $C_{2X}=0$ and $C_{2Y}=0$ are satisfied [6]. Then Eq. (2.30) leads to the following initial conditions for the collective variables [6]:

$$\dot{X}(0) = \frac{1}{\Delta t} \frac{[\epsilon_X + \epsilon_Y(M_{XY}/M_X)](1-b_Y) - \Gamma[\epsilon_X + \epsilon_Y(M_Y/M_{XY})](1-b_{XY})}{(1-b_X)(1-b_Y) - \Gamma(1-b_{XY})^2} , \tag{2.31}$$

$$\dot{Y}(0) = \frac{1}{\Delta t} \frac{[\epsilon_Y + \epsilon_X(M_{XY}/M_Y)](1-b_X) - \Gamma[\epsilon_Y + \epsilon_X(M_X/M_{XY})](1-b_{XY})}{(1-b_X)(1-b_Y) - \Gamma(1-b_{XY})^2} , \tag{2.32}$$

with

$$b_X = \frac{\langle f_{n,XX} | q_n \rangle}{M_X}, \quad b_Y = \frac{\langle f_{n,YY} | q_n \rangle}{M_Y} ,$$
$$b_{XY} = \frac{\langle f_{n,XY} | q_n \rangle}{M_{XY}}, \quad \Gamma = \frac{M_{XY}^2}{M_X M_Y} , \tag{2.33}$$

$$q_n(0) = Q_n(0) - f_n(X_0, Y_0) , \tag{2.34}$$

$$\dot{q}_n(0) = \left[\frac{\epsilon_X}{\Delta t} - \dot{X}(0) \right] f_{n,X}(X_0, Y_0) + \left[\frac{\epsilon_Y}{\Delta t} - \dot{Y}(0) \right] f_{n,Y}(X_0, Y_0) . \tag{2.35}$$

Thus the benefit of using the CV approach just described is that the physical meaning of the collective variables appears clearly, and one has exact explicit equations of motion for the collective modes for which the collective variables have been introduced. Moreover, this approach can allow for one to proceed quite far in some analytical investigations, as we will show in the following section, where we apply the CV equations of motion to the determination of some analytical expressions for the small-oscillation frequencies for the collective modes of the discrete DSG kink.

III. LOWEST-ORDER FREQUENCIES FOR THE COLLECTIVE MODES

We now focus on small-amplitude oscillations about the static DSG kink, and proceed with the determination of the lowest-order expressions for the frequencies of the collective modes X and Y, hereafter denoted as ω_X and ω_Y, respectively.

We determine ω_X in the small-amplitude limit by setting $Y=0$, assuming $\omega_0 \ll 1$, setting $q_n=0$ for all n, and neglecting the small terms of order $\dot{X}^2$. We call the approximation of setting $q_n=0$ the "bare approximation." Then Eq. (2.26) becomes

$$\ddot{X} = \frac{1}{M_X} \left[\langle f_{n,X} | \Delta_2 f_n \rangle - \omega_0^2 \left\langle f_{n,X} \left| \frac{dV_{\Re}[f_n(\xi_n, \Re)]}{df_n} \right\rangle \right] . \tag{3.1}$$

In the limit that $\omega_0 \ll 1$,

$$\Delta_2 f_n = f_{n+1} - 2f_n + f_{n+1} \approx \frac{d^2 f_n}{dn^2} + \frac{2}{4!} \frac{d^4 f_n}{dn^4} ,$$

where we neglect the terms higher than and including the sixth-derivative term. Then Eq. (3.1) becomes

$$\ddot{X} = \frac{1}{M_X} \frac{2}{4!} \langle f_{n,X} | f_{n,XXXX} \rangle . \tag{3.2}$$

In deriving Eq. (3.2) we have made use of the fact that $f_n(\xi_n, \Re)$ is the exact solution of the following equation:

$$\frac{\partial^2 f_n(\xi_n,\Re)}{\partial n^2}=\frac{\partial^2 f_n(\xi_n,\Re)}{\partial X^2}=\omega_0^2\frac{\partial V_\Re[f_n(\xi_n,\Re)]}{\partial f_n} . \quad (3.3)$$

When we expand a function of the form $\sum_n g(n-X)$ in a Fourier series we obtain

$$\sum_{n=-\infty}^{+\infty} g(n-X)=\frac{A_0}{2}+\sum_{n=1}^{+\infty} A_n\cos(2\pi nX) + \sum_{n=0}^{+\infty} B_n\sin(2\pi nX) , \quad (3.4)$$

where

$$A_n=2\int_{-\infty}^{+\infty} g(u)\cos(2\pi nu)du ,$$

$$B_n=-2\int_{-\infty}^{+\infty} g(u)\sin(2\pi nu)du, \quad n=0,1,\ldots . \quad (3.5)$$

We therefore find

$$M_X=M_{0_X}+\sum_{n=1}^{+\infty} A_{n_X}\cos(2\pi nX) , \quad (3.6)$$

where

$$M_{0_X}=16\omega_0\left[1+\frac{2\Re}{\sinh(2\Re)}\right] , \quad (3.7a)$$

$$A_{n_X}=\frac{16\omega_0}{\sinh(n\pi L_0/2)}\left[n\pi L_0\cos(nL_0\Re) + \frac{2\pi\sin(nL_0\Re)}{\sinh(2\Re)}\right] . \quad (3.7b)$$

Note that the dc term for the discrete mass, M_{0_X}, is in fact the continuum mass expression [2], and discreteness causes oscillation in X about the continuum value. Furthermore, we see in Eq. (3.7b) that the coefficients A_{n_X} decay exponentially as n increases, so that we can keep only the dc term in Eq. (3.6). Then Eq. (3.2) becomes

$$\ddot{X}=\frac{1}{12M_{0_X}}\sum_{n=1}^{+\infty} B_{n_X}\sin(2\pi nX) \quad (3.8)$$

where we obtain the coefficients B_{n_X} after relatively lengthy calculations:

$$B_{n_X}=\frac{8n\pi\omega_0^4}{\sinh(n\pi L_0/2)}\left[\frac{nL_0^2}{2}\cos(nL_0\Re)\left[n^2L_0^2+2+12\frac{\cosh(2\Re)}{\sinh^2(2\Re)}\right]+\frac{2L_0\sin(nL_0\Re)}{\sinh(2\Re)}\left[n^2L_0^2+3-\frac{6}{\tanh^2(2\Re)}\right]\right] . \quad (3.9)$$

Equation (3.9) shows that the coefficients B_{n_X} decay exponentially as n increases, so that one can keep only the $n=1$ term in Eq. (3.8), which gives us the following equation:

$$\ddot{X}=-\frac{\omega_X^2}{2\pi}\sin(2\pi X) , \quad (3.10)$$

where

$$\omega_X^2=\frac{2\pi^5}{3\sinh(\pi L_0/2)}\frac{1}{1+2\Re/\sinh(2\Re)}\left\{\frac{L_0}{2}\cos(L_0\Re)\left[1+\frac{2}{L_0^2}\left[1+6\frac{\cosh(2\Re)}{\sinh^2(2\Re)}\right]\right] + \frac{\sin(L_0\Re)}{\sinh(2\Re)}\left[2+\frac{6}{L_0^2}\left[1-\frac{2}{\tanh^2(2\Re)}\right]\right]\right\} \quad (3.11)$$

represents the square of the PN frequency of the DSG kink, to lowest order.

We now consider the determination of ω_Y, by assuming that the c.m. of the kink is held constant ($\ddot{X}=\dot{X}=0$) at an equilibrium point of the PN potential. Furthermore, in order to facilitate some forthcoming algebraic manipulations we make use of the variable [1]

$$R\equiv\Re+Y . \quad (3.12)$$

Then using the bare approximation, the CV equation of motion (2.27) becomes

$$\ddot{R}=\frac{1}{M_R}\left[\langle f_{n,R}|\Delta_2 f_n\rangle - \omega_0^2\left\langle f_{n,R}\left|\frac{\partial V_\Re[f_n(\xi_n,R)]}{\partial f_n}\right\rangle\right] , \quad (3.13)$$

where $M_R\equiv\langle f_{n,R}|f_{n,R}\rangle=\langle f_{n,Y}|f_{n,Y}\rangle$.

As we have done previously for calculating ω_X, we make again the following approximations:

$$\Delta_2 f_n\approx\frac{d^2 f_n}{dn^2}+\frac{2}{4!}\frac{d^4 f_n}{dn^4}$$

and

$$M_R = M_{0_Y} + \sum_{n=1}^{+\infty} A_{n_Y} \cos(2\pi n X) \approx M_{0_Y} , \tag{3.14}$$

where

$$M_{0_Y} = \frac{16}{\omega_0}\left[1 - \frac{2\Re}{\sinh(2\Re)}\right] . \tag{3.15}$$

Then Eq. (3.13) becomes

$$\ddot{R} = \frac{\omega_0^2}{M_{0_Y}}\left[\left\langle f_{n,R}\left|\frac{\partial^2 f_n(\xi_n,R)}{\partial n^2}\right\rangle - \left\langle f_{n,R}\left|\frac{\partial V_{\Re}[f_n(\xi_n,R)]}{\partial f_n}\right\rangle\right]\right. + \frac{1}{12M_{0_Y}}\left\langle f_{n,R}\left|\frac{\partial^4 f_n}{\partial n^4}\right\rangle\right. . \tag{3.16}$$

Furthermore, Eq. (3.3) implies that

$$\frac{\partial^2 f_n(\xi_n,R)}{\partial n^2} = \frac{\partial^2 f_n(\xi_n,R)}{\partial X^2} = \omega_0^2 \frac{\partial V_R[f_n(\xi_n,R)]}{\partial f_n} ,$$

so that Eq. (3.16) can be rewritten as follows:

$$\ddot{R} = \frac{\omega_0^2}{M_{0_Y}}\left[\left\langle f_{n,R}\left|\frac{\partial V_R[f_n(\xi_n,R)]}{\partial f_n}\right\rangle - \left\langle f_{n,R}\left|\frac{\partial V_{\Re}[f_n(\xi_n,R)]}{\partial f_n}\right\rangle\right]\right. + \frac{1}{12M_{0_Y}}\left\langle f_{n,R}\left|\frac{\partial^4 f_n}{\partial n^4}\right\rangle\right. , \tag{3.17}$$

where

$$V_R[f_n(\xi_n,R)] = 2\left[\frac{1}{\cosh(\xi_n+R)} + \frac{1}{\cosh(-\xi_n+R)}\right]^2 , \tag{3.18a}$$

$$V_{\Re}[f_n(\xi_n,R)] = \frac{8\cosh^2(R)\mathrm{sech}^2(\Re)}{\sinh^2(R)+\cosh^2(\xi_n)} + \frac{8\sinh^2(\xi_n)\sinh^2(\Re)}{[\sinh^2(R)+\cosh^2(\xi_n)]^2} . \tag{3.18b}$$

Performing analytically the summations in the first term of the right-hand side (RHS) of Eq. (3.17) is rather complicated. However, as we consider a system near the continuum limit, we can approximate those summations by an integration over the continuous position variable x; which leads to the following equation:

$$\ddot{R} = \frac{1}{M_{0_Y}}\frac{\partial \mathcal{V}(\Re,R)}{\partial R} + \frac{1}{12M_{0_Y}}\left\langle f_{n,R}\left|\frac{\partial^4 f_n}{\partial n^4}\right\rangle\right. , \tag{3.19}$$

where the function

$$\mathcal{V}(\Re,R) = \frac{1}{2}\omega_0^2 M_{0_Y}\left[\frac{\tanh^2(\Re)}{\tanh^2(R)} - \frac{\cosh^2(R)}{\cosh^2(\Re)}\right] + M_{0_X}\left[1+\frac{\cosh^2(R)}{\cosh^2(\Re)}\right] \tag{3.20}$$

was first derived in Ref. [1] for the study of the DSG kink dynamics in the continuum limit. When L_0 becomes sufficiently large—that is, in the continuum limit—the RHS of Eq. (3.19) reduces to the term $(1/M_{0_Y})[\partial\mathcal{V}(\Re,R)/\partial R]$. It was shown in Ref. [1] that in the continuum limit the expression of the frequency for small oscillations about $\Re$, to lowest order, is given by

$$\omega_{Y\text{-}C}^2 \equiv \left.\frac{1}{M_{0_Y}}\frac{\partial^2 \mathcal{V}(\Re,R)}{\partial^2 R}\right|_{R=\Re} = \frac{\omega_0^2}{1-2\Re/\sinh(2\Re)}\left[\frac{3-\Re/\tanh(\Re)}{\sinh^2(\Re)} + \frac{\Re\tanh(\Re)-1}{\cosh^2(\Re)} - \frac{2\Re}{\tanh(\Re)\sinh^2(\Re)\cosh^2(\Re)}\right] . \tag{3.21}$$

Thus Eq. (3.19) differs from the equation that we would have obtained if we were to carry out the same calculations in the continuum limit, by the presence of the term $\langle f_{n,R}|\partial^4 f_n/\partial n^4\rangle$ in the RHS of this equation. Note that this extra term is formally analogous to the term

$$\langle f_{n,X}|f_{n,XXXX}\rangle = \left\langle f_{n,X}\left|\frac{\partial^4 f_n}{\partial n^4}\right\rangle\right.$$

in the RHS of Eq. (3.2), whereas the term $(1/M_{0_Y})[\partial\mathcal{V}(\Re,R)/\partial R]$ [in Eq. (3.19)] has no equivalent in the RHS of Eq. (3.2). This is due to the fact that the c.m. mode of the kink becomes, in the continuum limit, the Goldstone mode ($\omega_{X\text{-in the continuum limit}} = \omega_{X\text{-}C} \equiv 0$).

Furthermore, as $\langle f_{n,R}|\partial^4 f_n/\partial n^4\rangle$ is an even and periodic function in X with period 1, we can expand it in a Fourier series:

$$\left\langle f_{n,R}\left|\frac{\partial^4 f_n}{\partial n^4}\right\rangle\right. = \frac{B_0}{2} + \sum_{n=1}^{+\infty} D_n \cos(2\pi n X) . \tag{3.22}$$

After relatively lengthy algebraic manipulations we obtain the following expression for the coefficients D_n:

$$D_n \equiv 2\int_{-\infty}^{+\infty}\left\langle f_{n,R}\left|\frac{\partial^4 f_n}{\partial n^4}\right\rangle\cos(2\pi nX)dX\right.$$
$$=\frac{-8\omega_0^4}{\sinh(n\pi L_0/2)\sinh(2R)}\left[nL_0^2\cos(nL_0R)\left[\frac{9}{2\tanh^2(2R)}-2\right]\right.$$
$$\left.+\frac{L_0\cosh(2R)\sin(nL_0R)}{\sinh(2R)}\left[\tfrac{3}{4}n^2L_0^2-\frac{9}{\sinh^2(2R)}-2\right]\right]. \tag{3.23}$$

Keeping only the first two terms of the series in Eq. (3.22) [since the coefficients decay as $1/\sinh(n\pi L_0/2)$], and expanding the second term in the RHS of Eq. (3.19) about $\Re$, we obtain the correction to $\omega_{Y\text{-}C}^2$ to lowest order, for small-amplitude oscillations:

$$\Omega^2=\frac{2\pi^5}{3L_0\sinh(\pi L_0/2)}\frac{\cos(2\pi X)}{1-2\Re/\sinh(2\Re)}\left\{-\cos(L_0\Re)\left[1+\frac{L_0^2}{2}+\frac{\cosh(2\Re)}{\sinh^2(2\Re)}\left[\frac{4}{L_0^2}+\frac{18}{L_0^2\sinh^2(2\Re)}-\frac{11}{2}\right]\right]\right.$$
$$\left.+\frac{L_0\sin(L_0\Re)}{\sinh(2\Re)}\left[2+\frac{1}{L_0^2}\left[4-\frac{9}{\tanh^2(2\Re)}\right]\right]\right\}. \tag{3.24}$$

Thus the frequency of small oscillations for the internal mode Y, to lowest order, is given by

$$\omega_Y^2=\omega_{Y\text{-}C}^2+\Omega^2 . \tag{3.25}$$

We should point out that the perturbation theory used above is only qualitatively correct [7]. The functional dependence of ω_X and ω_Y on the parameters is correct but fails to predict the correct numerical coefficients. The reason is that the dressing of the continuum kink shape due to discreteness contributes to ω_X and ω_Y to all orders of perturbation theory. However, we will show in the forthcoming discussion that ω_X and ω_Y are fortuitously very close to the exact values for $\Re>\Re_c$, where the meaning of $\Re_c$ will be made more precise later on.

We can check the accuracy of our lowest-order expressions for ω_X^2 and ω_Y^2 by performing numerically the exact determination of the small-oscillation spectrum of the kink system. To this end one must examine small oscillations in the system, in the presence of a stable DSG kink, $\Phi_n(X_{\rm eq})$, located at some equilibrium point $X=X_{\rm eq}$ of the PN potential. That is, we consider

$$Q_n(t)=\Phi_n(X_{\rm eq})+\vartheta_n(X_{\rm eq},t) ,$$

where

$$\vartheta_n(X_{\rm eq},t)=\epsilon\lambda_n(X_{\rm eq})\exp(-i\omega t) ,$$

ϵ is a small parameter, and $X_{\rm eq}\equiv m+\frac{1}{2}$, with m integer; that is, we focus on the case where the c.m. is located midway between two adjacent lattice sites.

The linearization of the equations of motion about $\Phi_n(X_{\rm eq})$ yields the following eigenvalue equation:

$$\mathcal{L}_{\rm DSG}\lambda_n=\omega^2\lambda_n , \tag{3.26}$$

where the linear operator $\mathcal{L}_{\rm DSG}$ is given by

$$\mathcal{L}_{\rm DSG}=\omega_0^2\left[\cos(\Phi_n)\tanh^2(\Re)-\frac{\cos(\Phi_n/2)}{\cosh^2(\Re)}-\Delta_2\right] . \tag{3.27}$$

Note that when $\Re$ becomes sufficiently large $\mathcal{L}_{\rm DSG}$ becomes $\mathcal{L}_{\rm SG}=\omega_0^2[\cos(\Phi_n)-\Delta_2]$, that is, the linear operator for the SG kink [8].

To calculate ω from the Eq. (3.26) we use the atomic positions in the stable kink state $\Phi_n(X_{\rm eq})$ (that we obtain via the classical pseudodynamics relaxation process). For a given parameter set $\{L_0,\Re\}$, the eigenvalue spectrum of Eq. (3.26) consists of a discrete set of traveling wave states (phonons) whose eigenvalues are given by the dispersion law

$$\omega_{k_n}^2=\omega_g^2+4\sin^2(k_n/2),\quad \omega_g^2=\omega_0^2[2\tanh^2(\Re)-1] , \tag{3.28}$$

where k_n is the wave vector associated with the frequency ω_{k_n}, and two bound states whose eigenvalues, $\omega^2<\omega_g^2$, give the exact small-oscillation frequencies for the collective modes X and Y.

Figures 2 and 3, obtained respectively for $L_0=10$ and 11, in the parameter range $1.3\le\Re\le 6.5$, show the variations of the frequencies $\{\omega_X(\Re),\omega_Y(\Re)\}$ (solid line) together with the exact determination of the frequencies of X and Y obtained via the linear operator $\mathcal{L}_{\rm DSG}$, hereafter referred to as "$\omega_{X\text{-exact}}$" and "$\omega_{Y\text{-exact}}$" respectively. We have also represented $\omega_{Y\text{-}C}/\omega_g$ versus $\Re$ (dotted curves) in Fig. 3. Note that the parameter regions where ω_X,ω_Y,

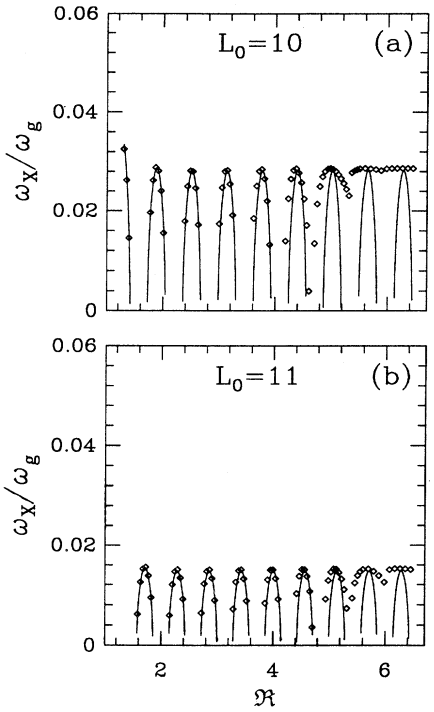

FIG. 2. Plot showing the normalized frequency of small oscillations of the c.m. mode ω_X/ω_g versus $\Re$, obtained from Eq. (3.11), for $L_0=$ (a) 10; (b) 11. The centers of the diamonds represent the exact determination obtained from the linear operator $\mathcal{L}_{\rm DSG}$.

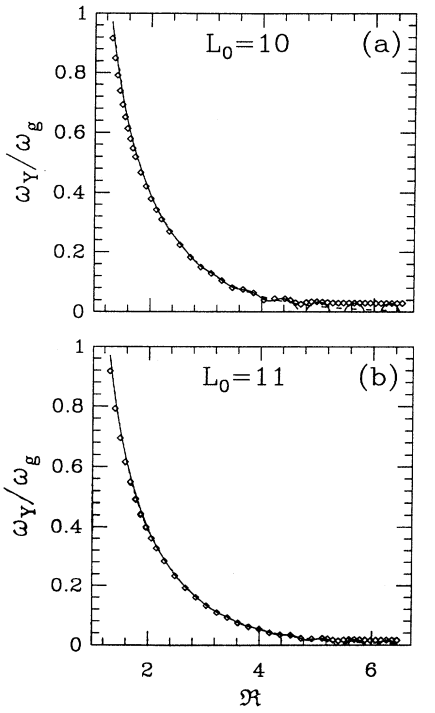

FIG. 3. Plot showing the normalized frequency of small oscillations of the internal mode ω_Y/ω_g versus $\Re$ (solid curve), obtained from Eq. (3.25), for $L_0=$ (a) 10; (b) 11. the dotted curve represents $\omega_{Y\text{-}C}(\Re)/\omega_g$, given by Eq. (3.21). The centers of the diamonds represent the exact determination, $\omega_{Y\text{-exact}}/\omega_g$.

or $\omega_{X\text{-exact}}$ are not represented in Figs. 2 and 3 correspond to the regions where the square of the frequency becomes negative. In particular, the regions where $\omega^2_{X\text{-exact}}<0$ correspond to the regions where the equilibrium position of the kink that we consider, $X_{\rm eq}=m+\frac{1}{2}$, becomes an unstable equilibrium point of the PN potential. Furthermore, we observe as general result that $\{\omega_X,\omega_Y\}$ agree more or less well with $\{\omega_{X\text{-exact}},\omega_{Y\text{-exact}}\}$ depending on the value of $\Re$ that one considers. Indeed we see in Figs. 2 and 3 that there exists a particular value of $\Re$ below which $\{\omega_X,\omega_Y\}$ agree surprisingly well with $\{\omega_{X\text{-exact}},\omega_{Y\text{-exact}}\}$. This value of $\Re$ is hereafter denoted "$\Re_c(L_0)$." Note that $\Re_c(10)\approx 3.4$, and $\Re_c(11)\approx 3.8$. Furthermore, we observe in Fig. 3 that $\omega_{Y\text{-}C}$ agree also very well with $\omega_{Y\text{-exact}}$ for $\Re\le\Re_c$.

On the other hand, from $\Re\approx\Re_c$ upwards, we observe that $\{\omega_X,\omega_Y\}$ no longer agree with $\{\omega_{X\text{-exact}},\omega_{Y\text{-exact}}\}$, for most values of $\Re$. Moreover, we have found out that in some small regions of $\Re$, above $\Re_c$, the square of the frequencies, ω^2_X and ω^2_Y, become negative, whereas both $\omega^2_{X\text{-exact}}$ and $\omega^2_{Y\text{-exact}}$ become essentially constant. A clear discrepancy also appears between $\omega_{Y\text{-}C}$ and $\omega_{Y\text{-exact}}$ when $\Re\ge\Re_c$, for $L_0=10$ [see Fig. 3(a)], but the discrepancy disappears progressively as L_0 increases, as shown in Fig. 3(b). A careful examination of the results for $\Re\ge\Re_c$ reveals some interesting features that allow one to gain more insight into the reasons for which the discrepancy appears for most values of $\Re$ in the range $\Re\ge\Re_c$. Indeed, the data for Figs. 2 and 3 indicate that when $\Re$ becomes sufficiently large ($\Re\ge\Re_c$) both $\omega_{X\text{-exact}}$ and $\omega_{Y\text{-exact}}$ tend asymptotically to the same constant that is precisely the value of the small-oscillation frequency of the c.m. of the SG kink, given by the linear operator $\mathcal{L}_{\rm SG}$. This means that when the parameter $\Re$ of the DSG potential becomes sufficiently large ($\Re\ge\Re_c$) the two subkinks of the DSG kink behave, with regard to small-amplitude oscillations, rather like two isolated SG kinks embedded in the same discrete lattice. Consequently, any bona fide analytical formula—intended to describe small oscillations in the DSG kink—must preserve this essential feature. In the limit of large $\Re$, in the case where the DSG kink is centered midway between two adjacent lattice sites ($X=m+\frac{1}{2}$), Eqs. (3.11) and (3.25) become, respectively,

$$\omega^2_X\approx\frac{\pi^5 L_0}{3\sinh(\pi L_0/2)}\left[1+\frac{2}{L_0^2}\right]\cos(L_0\Re)$$
$$=\omega^2_{\rm SG}\cos(L_0\Re)$$
$$=\frac{\pi^5 l_0}{3\sinh(\pi l_0)}\left[2+\frac{1}{l_0^2}\right]\cos(2l_0\Re),\quad l_0\equiv L_0/2\ , \tag{3.29}$$

$$\omega^2_Y\approx\Omega^2\approx\omega^2_{\rm SG}\cos(L_0\Re)\ , \tag{3.30}$$

where the factor $\omega^2_{\rm SG}$ represents precisely the small-oscillation frequency of the c.m. of the discrete SG kink, to lowest order [9] [we have introduced the variable l_0 just to facilitate comparison with Eq. (4.6) in Ref. [9]].

Equations (3.29) and (3.30) show that the $\Re$ dependence still exists in our expressions of $\{\omega_X^2,\omega_Y^2\}$ in the large-$\Re$ limit, owing to the presence of the factor $\cos(L_0\Re)$, whereas both $\omega_{X\text{-exact}}$ and $\omega_{Y\text{-exact}}$ tend asymptotically to ω_{SG}. This indicates that the ansatz function f_n that we have used for calculating $\{\omega_X,\omega_Y\}$ does not lead to the exact *limit behavior* for sufficiently large $\Re$, in a discrete lattice. Then it becomes clear that for suitably describing the behavior of the DSG kink, for large $\Re$ in a discrete lattice, one can still use the ansatz function that we have considered, provided that the discreteness parameter L_0 is chosen in such a way that $\cos(L_0\Re)=1$, that is,

$$L_0=L_{0_m}\equiv 2m\pi/\Re \quad \text{with } m \text{ integer} . \tag{3.31}$$

In order to understand the physical meaning of the relation (3.31) it is helpful to invoke Eqs. (2.14a) and (2.14b), which indicate that when $Y\approx 0$ the centers of the subkinks of the static DSG kink are located, respectively, at

$$X_1=X-\frac{L_0\Re}{2\pi} \quad \text{and} \quad X_2=X+\frac{L_0\Re}{2\pi} . \tag{3.32}$$

Then when one applies the relation (3.31) in Eq. (3.32) one obtains

$$X_1=X-m \quad \text{and} \quad X_2=X+m . \tag{3.33}$$

Equation (3.33) indicates that the distance between the two subkinks in the static DSG kink is then exactly equal to an integer number of periods of the lattice, thus implying that the two subkinks are located exactly at the same equilibrium point in the PN potential [we recall in this respect that the PN potential is a periodic potential, whose periodicity is equal to (or is twice as big as) [6] the one of the lattice]. If, in addition, the parameter $\Re$ of the potential becomes sufficiently large the subkinks will no longer overlap and will behave like two isolated kinks. As the square of the PN frequency is closely related to the curvature of the PN potential at the equilibrium point of the static kink [8], the subkinks will oscillate with the same frequency (since they are located exactly at the same equilibrium point in the PN potential). In this respect we observe in Figs. 2 and 3 the striking behavior that for some particular values of $\Re$, still above $\Re_c$, an excellent agreement appears again between $\{\omega_X,\omega_Y\}$ and $\{\omega_{X\text{-exact}},\omega_{Y\text{-exact}}\}$. Those values of $\Re$ correspond precisely to those that satisfy the relation Eq. (3.31).

Figs. 4 and 5, which show the plots of $\{\omega_X,\omega_Y\}$ versus L_0—where L_0 satisfies the relation Eq. (3.31)—exhibit two types of behavior: the *discrete regime* in which the frequencies vary strongly as a function of the discreteness parameter L_0, and the continuum limit (which manifests itself when L_0 becomes sufficiently large), in which the frequencies become constant with respect to L_0. We see in Figs. 4 that in the continuum limit ω_X is equal to zero and independent of $\Re$; which indicates that the c.m. mode becomes effectively the Goldstone mode. Furthermore, we see in Figs. 4 and 5 that discreteness effects begin to manifest themselves when $10\le L_0\le 11$; which shows that the values $L_0=10$ and 11 that we considered previously for obtaining the results in Figs. 2 and 3 correspond effectively to the case where discreteness effects are not too large.

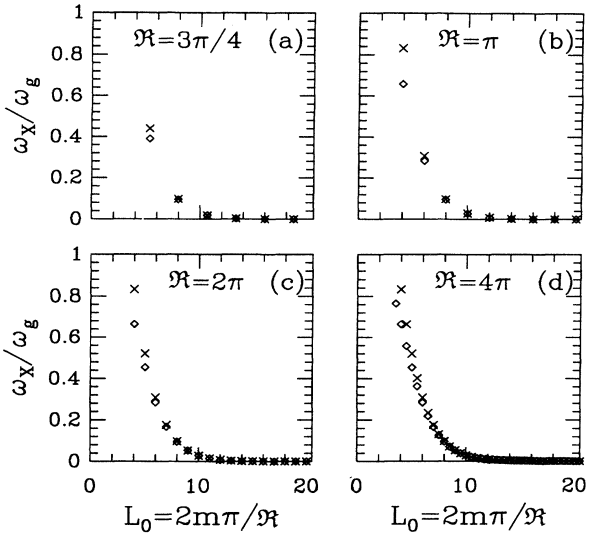

FIG. 4. The crosses represents the normalized small-oscillation frequency ω_X/ω_g versus $L_0=2m\pi/\Re$ (with m integer), obtained from Eq. (3.11). The diamonds represent the exact determination, $\omega_{X\text{-exact}}/\omega_g$. $\Re=$ (a) $3\pi/4$; (b) π; (c) 2π; (d) 4π.

The most striking point which emerges from our results in Figs. 4 and 5 is that from $L_0\approx 3\pi$—where discreteness effects begin to become important—up to the continuum limit our analytical expressions $\{\omega_X,\omega_Y\}$ agree surprisingly well with $\{\omega_{X\text{-exact}},\omega_{Y\text{-exact}}\}$. This ex-

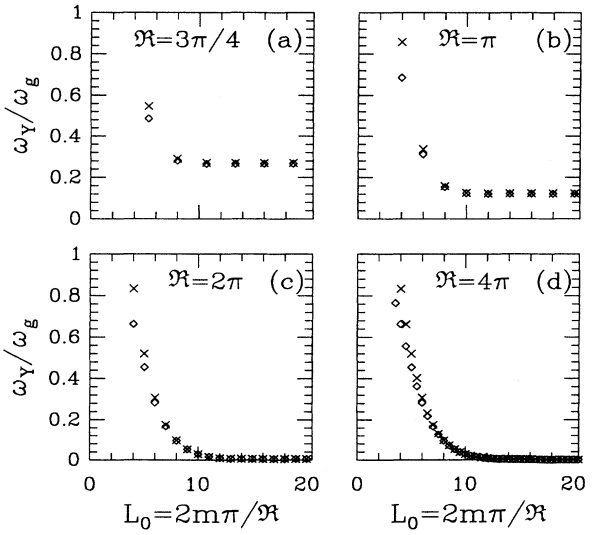

FIG. 5. The crosses represent the normalized small-oscillation frequency ω_Y/ω_g versus $L_0=2m\pi/\Re$ (with m integer), Eq. (3.25). The diamonds represent the exact determination, $\omega_{Y\text{-exact}}/\omega_g$. $\Re=$ (a) $3\pi/4$; (b) π; (c) 2π; (d) 4π.

cellent agreement is certainly due to the fact that the ansatz function f_n, that we have used for calculating $\{\omega_X,\omega_Y\}$, provides a highly accurate representation of the shape of the discrete DSG kink when discreteness effects are not too large. On the other hand, we observe, as one could expect, a clear discrepancy between $\{\omega_X,\omega_Y\}$ and $\{\omega_{X\text{-exact}},\omega_{Y\text{-exact}}\}$ when discreteness effects become too large ($L_0 \ll 3\pi$). Indeed, in the highly discrete regime, the bare approximation is no longer valid because the ansatz function f_n no longer represents the configuration of the discrete kink as well as in the former case. Consequently, in the highly discrete system, one needs to perform the static dressing of the kink by taking into account the q_n's, Eq. (2.8). In the following section we numerically solve the CV equations of motion (2.26), (2.27), and (2.28), where the q_n's are fully taken into account.

IV. NUMERICAL SOLUTIONS OF THE CV EQUATIONS OF MOTION

For performing the numerical computations, the total number of particles in the chain, N, will be chosen such that we do not encounter phonons reflected from the ends of the system. We will always choose the time step Δt and the total time for the dynamics in such a way that the magnitude of the constraints, Eq. (2.15), never exceeds 10^{-5}, and the energy of the system is conserved to an accuracy better than 0.01%. Furthermore, throughout the present paper, we consider the same discreteness parameter as in Ref. [10], that is, $L_0=5.588$, in order to facilitate the comparison between the behavior of the SG and DSG kink systems (in this respect, note that the discreteness parameter used in Ref. [10] is $l_0=L_0/2$, instead of L_0, so that our $L_0=5.588$ corresponds exactly to the value of $l_0=2.794$ used in Ref. [10] where the authors examined a discrete SG kink).

For our numerical solutions of the CV equations of motion, we consider two different kink profiles corresponding to two different values of $\mathfrak{R}$; first we consider the value of $\mathfrak{R}$ such that the distance between the subkinks is so large that the subkinks do not overlap, and second the case where $\mathfrak{R}$ is so small that the subkinks overlap and lose their individual identities. In order for the results to be conveniently displayed we discuss the two cases separately.

A. Kink dynamics for $\mathfrak{R}=26\pi/L_0 \approx 14.617$

The chosen parameter $\mathfrak{R}=26\pi/L_0$ gives rise to a DSG kink where the centers of the subkinks are separated by $\mathcal{D}=2\mathfrak{R}/\omega_0=26$ lattice cells, for $Y=0$. Thus the separation between the subkinks is large compared with the size of each subkink as can be seen in Fig. 6 (obtained via the relaxation process), which shows the static profile of a discrete DSG kink located midway between two adjacent lattice sites. This figure shows effectively that the subkinks do not overlap for the value of $\mathfrak{R}$ that is considered. Consequently, one can consider, in some respects, that each subkink is embedded in a PN potential in the same manner as is a single kink in the discrete SG system;

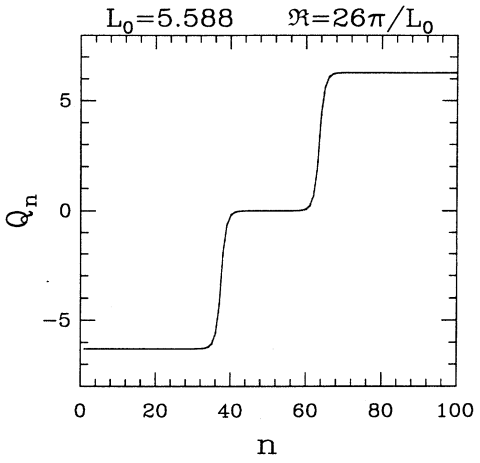

FIG. 6. Profile of the discrete DSG kink, centered at $X=50.5$ in a 100 particle chain, for $L_0=5.588$ and $\mathfrak{R}=26\pi/L_0$.

which implies that the stable equilibrium point of each subkink inside its PN potential is located midway between two adjacent lattice sites, as schematically shown in Fig. 7(a), where

$$X_1=X_{1\text{eq}}\equiv m_1+\tfrac{1}{2},\quad X_2=X_{2\text{eq}}\equiv m_2+\tfrac{1}{2}\ , \tag{4.1}$$

and m_1 and m_2 are integers.

Then Eqs. (2.14) yield the equilibrium values for the collective modes associated with the whole DSG kink:

$$X=X_{\text{eq}}\equiv\frac{X_{1\text{eq}}+X_{2\text{eq}}}{2}=\frac{m_1+m_2}{2}+\tfrac{1}{2}\ , \tag{4.2a}$$

$$Y=Y_{\text{eq}}\equiv\frac{\omega_0(X_{2\text{eq}}-X_{1\text{eq}})}{2}-\mathfrak{R}=\frac{\omega_0(m_2-m_1)}{2}-\mathfrak{R}\ . \tag{4.2b}$$

For performing the kink dynamics, one must first obtain an initial kink profile $Q_n(t=0)$ (via the relaxation process) in which at least one of the subkinks is away from its equilibrium point in the PN potential, that is,

$$X_1(t=0)=m_1+\xi_1,\quad X_2(t=0)=m_2+\xi_2\ , \tag{4.3}$$

where $0\le\xi_1<1$, $0\le\xi_2<1$, but with $\xi_1\neq\frac{1}{2}$ or $\xi_2\neq\frac{1}{2}$. The parameters ξ_1 and ξ_2 therefore locate, respectively, the positions of the two subkinks inside their PN potentials. The initial conditions for X and Y are then written, respectively,

$$X(t=0)=\frac{X_1(t=0)+X_2(t=0)}{2}=X_{\text{eq}}+\frac{\xi_1+\xi_2-1}{2}\ , \tag{4.4}$$

$$Y(t=0)=\frac{\omega_0[X_2(t=0)-X_1(t=0)]}{2}-\Re$$
$$=Y_{\rm eq}+\frac{\omega_0(\xi_2-\xi_1)}{2}\ . \tag{4.5}$$

Thus a set of ξ_1 and ξ_2 values, associated with the initial velocities for the CV, or equivalently the initial velocities on the particles, make up a type of initial conditions for the dynamics. Figures 7(b)–7(d) show schematically the different types of initial topological conditions that we will consider later on. Figure 7(b) corresponds to a case where the subkinks are initially deviated by the same amplitude in opposite directions, from their stable equilibrium points in their respective PN potentials; which corresponds to an initial excitation of the internal mode Y keeping the c.m. at equilibrium $[X(t=0)=X_{\rm eq}]$. In Fig. 7(c) the two subkinks are deviated by the same amplitude in the same direction, from their stable equilibrium points in the PN potential; which corresponds to an excitation of the c.m. X whereas $Y(t=0)=Y_{\rm eq}$. Figure 7(d) corresponds to a case where the two collective modes X and Y are initially excited.

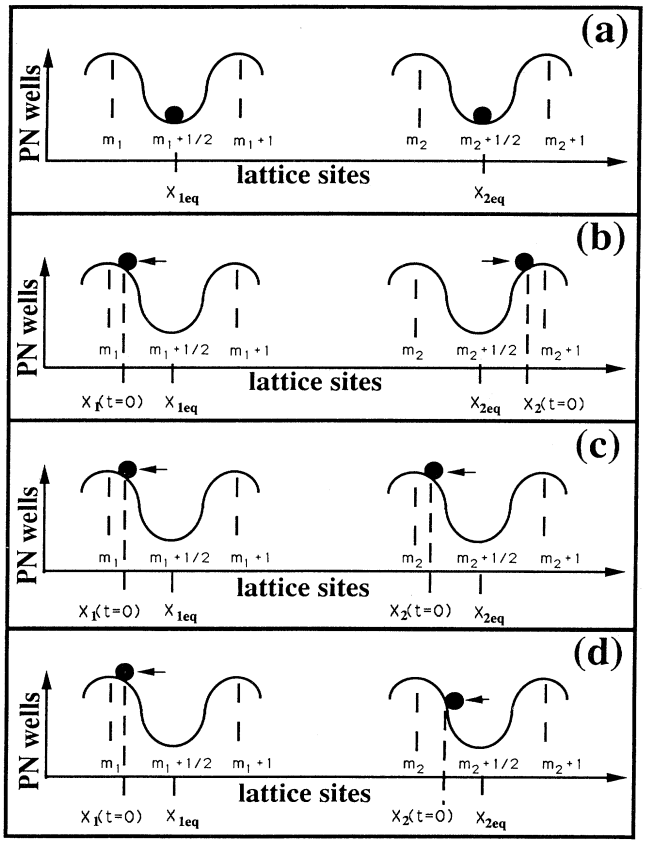

FIG. 7. Schematic representation of some possible positions of the subkinks inside their individual PN potentials, when the parameter $\Re$ becomes sufficiently large. m_1 and m_2 are integers which designate, respectively, the lattice sites situated near the subkinks. (a) corresponds to the equilibrium state of the DSG kink, whereas (b) and (c) correspond to various excited states. Note, however, that the shape of the PN potential experienced by each subkink is very close but not exactly identical to the one of a single SG kink because the subkinks in the DSG system are always bound via the parameter $\Re$, even when the separation between the subkinks becomes sufficiently large.

For each of these initial topological configurations, it remains to choose the initial velocities in order to completely determine the type of initial conditions for the specific type of dynamics that one desires (trapped or untrapped regime). We discuss separately the trapped or untrapped regimes of the kink.

1. *The trapped regime for* $\Re=26\pi/L_0$

We first examine the trapped regime of the kink by choosing the initial velocities on the particle to be zero, that is, $\dot{Q}_n(t=0)=0$; which corresponds, for the CV theory, to $\epsilon_X=\epsilon_Y=0$, or equivalently,

$$\dot{X}(t=0)=0,\quad \dot{Y}(t=0)=0\ . \tag{4.6}$$

a. Kink dynamics corresponding to the initial excitation of Y. Figure 8 shows the results obtained for a 3000-particle chain, where the subkinks were initially deviated from their stable equilibrium positions, as schematically shown in Fig. 7(b), precisely in the following way:

$$X_1(t=0)=1487.017\,960\,4=X_{1\rm eq}-0.482\,04\ ,$$
$$X_2(t=0)=1513.982\,04=X_{2\rm eq}+0.482\,04\ ; \tag{4.7a}$$

which corresponds, for the whole system, to

$$X(t=0)=1500.5=X_{\rm eq},\quad Y(t=0)=0.542\,01\quad (Y_{\rm eq}=0)\ . \tag{4.7b}$$

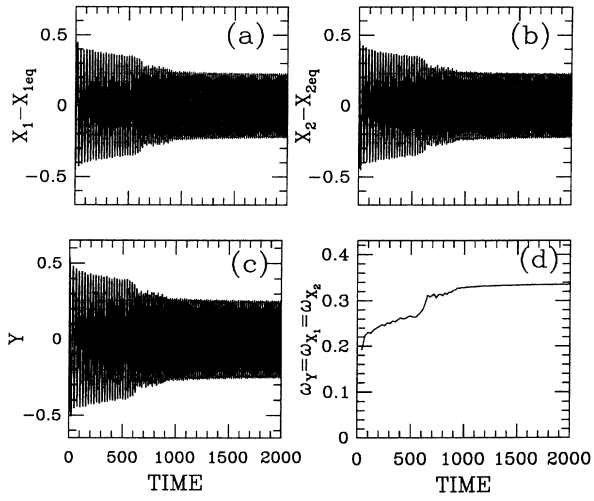

FIG. 8. Kink dynamics for an initial excitation of the internal mode Y, that leads to the trapped regime, for $L_0=5.588$ and $\Re=26\pi/L_0$. (a) $X_1(t)-X_{1\rm eq}$; (b) $X_2(t)-X_{2\rm eq}$; (c) $Y(t)$; (d) $\omega_Y(t)=\omega_{X_1}(t)=\omega_{X_2}(t)$. $X_{1\rm eq}=1487.5$ and $X_{2\rm eq}=1513.5$. Simulation parameters are $\epsilon_X=\epsilon_Y=0$, $\Delta t=\pi/114.7$, and $N=3000$.

Equation (2.29) yields $Z=1.033\,52$.

As a general result we find that the centers of the two subkinks vibrate with the same amplitude of oscillations but with opposite velocities, so that the c.m. of the whole DSG kink remains at equilibrium during the dynamics: $X(t)=X(t=0)=X_{eq}$. Consequently, only one of the two collective modes of the system is excited during the dynamics and vibrates with frequency $\omega_Y(t)=\omega_{X_1}(t)=\omega_{X_2}(t)$. Figures 8(a) and 8(b) show that as soon as the dynamics begins the amplitude of oscillation for each subkink decreases monotonically and smoothly, thus implying that the subkink is loosing energy via the phonons radiation process, up to $t=643$ where a drop occurs in the amplitude of oscillation. This drop is a clear and strong manifestation of the general process that involves the spontaneous emission of phonon radiation, reported in Ref. [10]. This process involves a coupling of the nonlinear collective mode to the phonon modes. The nonlinear collective mode possesses a fundamental frequency which lies generally below the lower phonon band edge. This fundamental frequency increases in time (due to the loss of energy of the collective mode), and so do its harmonics, so that when a harmonic that was initially below the lower phonon band edge crosses up into the phonon band it resonates with phonon modes and then the kink emits a burst of phonon radiation. Since the kink loses energy through radiation of phonons the amplitude of the oscillations decreases and the frequency of the oscillations increases. In the beginning of the motion, from $t=0$ up to $t=643$, the kink radiates away phonons owing to higher harmonics of the frequency $\omega_Y=\omega_{X_1}=\omega_{X_2}$ which enter the phonon band, but the individual effect of each of those harmonics is not yet sufficiently strong to manifest itself clearly. On the other hand, at $t=643$, the individual effect of a harmonic become clearly appreciable, as shown in Fig. 8(d), where the frequency $\omega_Y=\omega_{X_1}=\omega_{X_2}$ jumps suddenly from $\omega_Y=0.281=\omega_g/4$ to about $\omega_Y=0.31$; which indicates that the drop in the amplitude of oscillation of each subkink is due the fourth harmonic of $\omega_Y=\omega_{X_1}=\omega_{X_2}$ that crosses up into the phonon band. The behavior just described corresponds precisely to the same general features as those reported in Ref. [10] for a discrete SG kink. There exist, however, some qualitatively different features between a subkink of the DSG system and a single SG kink, that we now point out.

A careful examination of our Figs. 8(a) and 8(b) reveals a slight difference with respect to the result in Fig. 3(a) in Ref. [10], after the drop in the amplitude of oscillation of each subkink. Indeed we observe in Figs. 8(a) and 8(b) that after the drop the amplitude of oscillation of each subkink increases very slightly for a few oscillations before decreasing monotonically. This slight increase in the amplitude of oscillation indicates that each subkink absorbs and reemits a relatively important packet of energy just after the emission of the burst of phonon radiation. Such a phenomenon, which does not occur in the SG kink system [10], is due to the configuration of the DSG kink; indeed, as each subkink always radiates away phonons in both directions (in the positive and negative x directions) it is clear that a relatively important part of the energy radiated by each subkink must pass through the other subkink before being radiated away from the two subkinks; hence the slight increase in the amplitude of each subkink after the drop at $t=643$.

It is interesting to mention that one can also analyze the behavior just described by simply regarding the DSG kink as a whole collective entity described solely by the internal mode (IM) Y. In this context, the drop at $t=643$ in the amplitude of oscillation of Y in Fig. 8(c), followed by the slight increase, indicates that a packet of the energy of the Y mode is transferred to the phonon modes as the fourth harmonic of ω_Y enters the phonon band, and, just after, a part of the energy lost by Y is transferred back to Y before being ultimately radiated away from the kink. Consequently, this behavior can well be regarded as a sort of energy-exchange process that temporarily occurs between the IM Y and the phonon modes when a burst of phonons is emitted by the kink.

b. Kink dynamics corresponding to the initial excitation of the c.m. X. Figure 9 shows the results obtained for a 3000 particle chain, where the subkinks are initially deviated in the same direction from their stable equilibrium positions [as schematically shown in Fig. 7(c)], precisely in the following way:

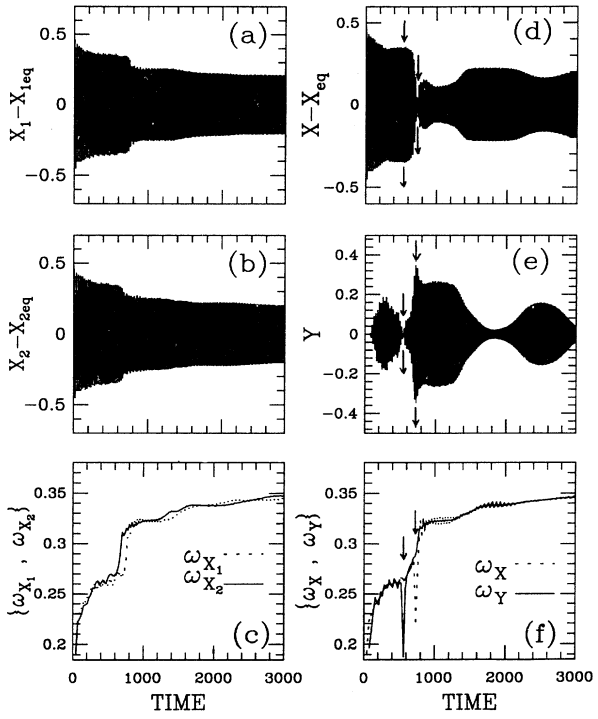

FIG. 9. Kink dynamics for an initial excitation of the c.m. mode X, that leads to the trapped regime, for $L_0=5.588$ and $\Re=26\pi/L_0$. (a) $X_1(t)-X_{1eq}$; (b) $X_2(t)-X_{2eq}$; (c) $\omega_{X_1}(t)$ and $\omega_{X_2}(t)$; (d) $X(t)-X_{eq}$; (e) $Y(t)$; (f) $\omega_X(t)$ and $\omega_Y(t)$. $X_{1eq}=1500.5$. Simulation parameters are $\epsilon_X=\epsilon_Y=0$, $\Delta t=\pi/114.7$, and $N=3000$.

$$X_1(t=0)=1487.984\,036=X_{1eq}+0.484\,036\ ,$$
$$X_2(t=0)=1513.984\,036=X_{2eq}+0.484\,036\ ; \tag{4.8a}$$

which corresponds to

$$X(t=0)=1500.984\,036=X_{eq}+0.484\,036\ ,$$
$$Y(t=0)=0=Y_{eq}\ . \tag{4.8b}$$

Equation (2.29) yields $Z=1.033\,809\,3$. Furthermore, we recall that the initial velocities on the particles are chosen to be zero.

Figures 9(a) and 9(b) show that a significant drop appears in the amplitude of oscillation of each subkink, owing to the fourth harmonic of the frequency of oscillation of the center of each subkink, that enters the phonon band. This shows that the phonon-radiation process still plays an important role in the dynamics. However, the kink dynamics now differ qualitatively from the previous case owing to the fact that although the IM Y is not initially excited, this mode ends up by moving from its equilibrium position, and executes, later on, a relatively large-amplitude motion, as shown in Fig. 9(e). So there exists a fundamental difference between the previous case (Sec. IV A 1 a) where the c.m. mode remains at equilibrium throughout the dynamics when only the IM Y is initially excited, and the present case where the IM Y ends up by moving from equilibrium when only the c.m. mode X is initially excited. Indeed the initial excitation of Y [Fig. 7(b)] preserves the symmetry of the system with respect to the c.m. of the system, so that during the dynamics the phonons are radiated away from the kink exactly in the same manner in the positive and negative x directions. In this case the phonons cannot act as a source of excitation of the c.m. On the other hand, the initial excitation of X [Fig. 7(c)] breaks down the symmetry of the system with respect to the positive and negative x directions, and in consequence, the phonons are no longer radiated away from the kink exactly in the same manner in the two directions. The phonons emitted by the kinks therefore act a source of excitation which ends up by setting progressively the internal mode in motion at $t\approx 100$ [Fig. 9(e)].

Furthermore, we observe in Figs. 9(d) and 9(e) that X and Y always evolve in time in a cooperative way in the sense that the amplitudes of oscillation of X and Y always vary inversely, so that each mode attains its maxima precisely as the other mode attains its minima, and vice versa. This cooperative motion indicates in fact that when X and Y are both excited, an energy-exchange process occurs permanently between these two modes in the discrete DSG kink. During this energy-exchange process, it sometimes happens that one mode loses almost all its energy during a short lapse of time; which leads to a significant drop in its frequency of oscillation. This behavior is indicated by down arrows in Figs. 9(d)–9(f).

On the other hand, by carefully looking into Figs. 9(c)–9(e), we have found that as long as $\omega_{X_1}(t)\neq\omega_{X_2}(t)$ an energy transfer occurs between X and Y, and each time that $\omega_{X_1}(t)$ becomes equal to $\omega_{X_2}(t)$, X and Y attain their extrema; that is, the transfer of energy from one mode to the other stops and begins again, but in the opposite direction.

The following point should also be mentioned: since each subkink radiates a part of its energy in the direction of the other subkink, we would expect there to be a slight increase in the amplitude of oscillation of each subkink, immediately after the drop due to the emission of a burst of phonons, in a similar way as in the case of Figs. 8(a) and 8(b). On the other hand, we do effectively observe some slight increases after the drop in the amplitudes of X_1 and X_2 in Figs. 9(a) and 9(b), but they appear later than in the case of Figs. 8(a) and 8(b). We attribute this slight difference to the fact that the dynamics, in the case of Figs. 9(a) and 9(b), are no longer governed solely by the phonon-radiation process, but also by the energy-exchange process between X and Y. So all phonons emitted by each subkink are not radiated directly from the DSG kink; some of them interfere with the energy-exchange process between X and Y, before being ultimately radiated away later on.

c. Initial excitation of X and Y. We have performed the kink dynamics in the case where the subkinks are initially deviated in the same direction, but with different amplitudes, from their stable equilibrium positions [in a similar way as in Fig. 7(d)]. We have found that both X and Y begin to move as soon as the dynamics begin, but the important point that we have noticed is that the kink dynamics are still governed by the same physical processes already described previously in the case of Fig. 9, namely, the phonon-radiation process and the energy-exchange process between X and Y. Since this behavior has already been discussed in detail in the previous subsection, we do not show the figures in the present subsection. We now turn to the untrapped regime of the kink.

2. *The untrapped regime for $\Re=26\pi/L_0$*

We consider again a DSG kink where the subkinks are initially deviated from their stable equilibrium positions exactly in the same way as in Sec. IV A 1 b, but in a 2000 particle chain. For obtaining the untrapped regime we put an initial velocity on the c.m. X of the whole DSG kink, by choosing

$$\epsilon_X=-0.005\,25,\quad \epsilon_Y=0\ , \tag{4.9a}$$

which corresponds to

$$\dot{X}(t=0)=V_{X_1}(t=0)\equiv\dot{X}_1(t=0)$$
$$=V_{X_2}(t=0)\equiv\dot{X}_2(t=0)$$
$$=-0.191\,151\,395\ . \tag{4.9b}$$

Figure 10(a) shows that the discrete DSG kink exhibits all regimes of a discrete kink motion: the untrapped regime in which the kink ballistically propagates in the lattice while emitting radiation, and the trapped regime which occurs when the kink has lost enough energy. We see in Fig. 10(b) that, although the Y mode is not initially excited, this mode becomes excited at about $t=60$, owing

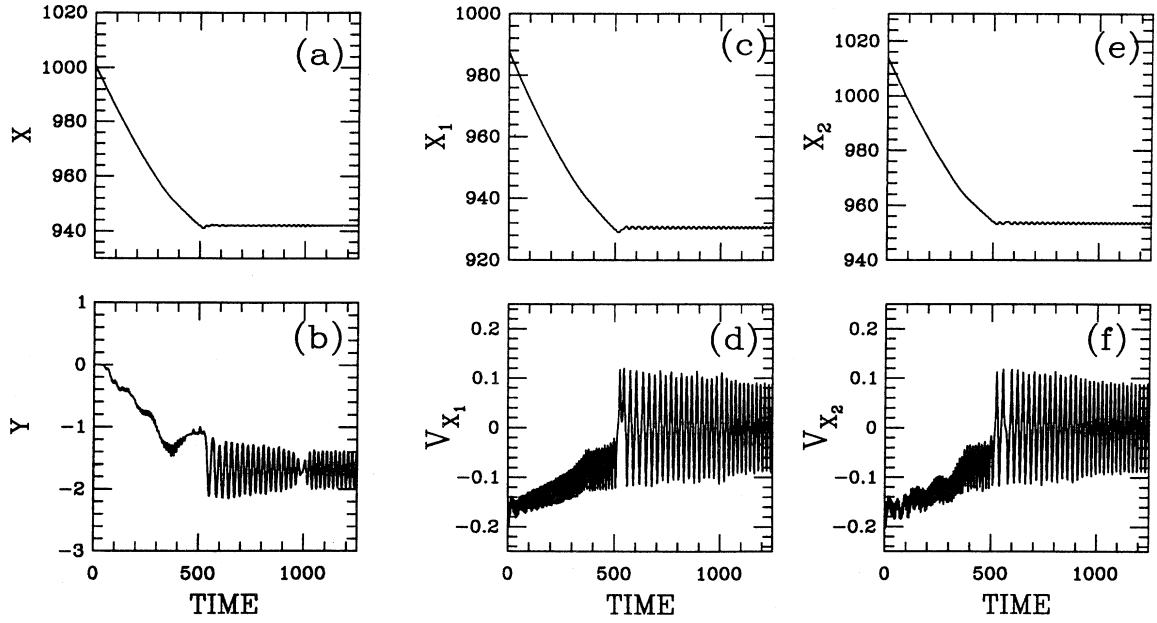

FIG. 10. Kink dynamics for an initial excitation of the c.m. mode X, that leads to the untrapped regime, for $L_0=5.588$ and $\Re=26\pi/L_0$. (a) $X(t)$; (b) $Y(t)$; (c) $X_1(t)$; (d) $V_{X_1}(t)$; (e) $X_2(t)$; (f) $V_{X_2}(t)$. Simulation parameters are $\epsilon_X=-0.005\,25$, $\epsilon_Y=0$, $\Delta t=\pi/114.7$, and $N=2000$.

to the phonons emitted which act as a source of excitation. So from $t=0$ up to $t\approx 60$ the DSG kink behaves exactly like a train of two subkinks which are tightly bound, which travel through the lattice in the negative x direction with essentially the same velocity. The subkink at the front of the train, located by X_1, Fig. 10(c), will be hereafter referred to as the "forward subkink," whereas the subkink in the rear of the train, located by X_2, Fig. 10(e), will be referred to as the "backward subkink." Furthermore, we see in Fig. 10(b) that in the beginning of the Y mode motion its amplitude decreases continually up to $t\approx 375$, thus indicating that the backward subkink is moving faster than the forward subkink, since the separation between the subkinks, Eq. (2.14c), is closely related to Y. Then from $t\approx 375$ onwards Y increases until the kink becomes trapped. After the transition to the trapped regime, the Y mode oscillates about $\langle Y(t)\rangle=-1.7$.

Thus we find the surprising result that the dynamics in the untrapped regime ends up by modifying permanently the distance between the subkinks of the DSG system. In the beginning of the dynamics, $Y[0\le t\le 60]\approx 0$, so that the distance between the subkinks is

$$\mathcal{D}_{\text{initial}}\equiv\mathcal{D}(t=0)=2\Re/\omega_0=26 \text{ lattice cells} .$$

But after the transition to the trapped regime the mean value of the distance between the subkinks becomes

$$\mathcal{D}_{\text{final}}=\langle\mathcal{D}(t)\rangle=2[\Re+\langle Y(t)\rangle]/\omega_0$$
$$=2(\Re-1.7)/\omega_0\approx 23 \text{ lattice cells} .$$

This permanent modification of the kink profile is one of the most outstanding effects of the phonon-radiation process on the behavior of the discrete DSG kink. In this respect it should be mentioned that the phonon-radiation process, in the untrapped regime, manifests itself in a somewhat different way than in the trapped regime.

Indeed, one of the main results of previous work [10,11] on discreteness effects in kink-bearing systems is that the ballistic propagation of the kink give rise to a periodic excitation of the lattice, whose fundamental frequency corresponds to the frequency with which the kink passes the sites of the lattice; that is,

$$\Omega=2\pi\dot{X} , \tag{4.10}$$

or equivalently

$$\Omega_1=2\pi\dot{X}_1,\quad \Omega_2=2\pi\dot{X}_2 ,$$

when one considers rather the frequency with which each subkink passes the sites of the lattice. The phonon radiation in the untrapped regime is due to the presence of Ω, or any of its harmonics, in the phonon band. During the untrapped regime the kink velocity decreases in time, and so do Ω and its harmonics, and when a harmonic that was initially inside the phonon band pass out through the bottom of the phonon band this harmonic becomes incapable of producing radiation. This physical process leads to knees in the curves of the kink's velocity versus time [11], which appear at critical velocities, at which the radiation rate drops significantly. One of these velocities is clearly visible in Figs. 10(d) and 10(f) at $t\approx 375$, where

$$V_{X_1}=V_{X_2}=-0.0447=\tfrac{1}{4}(\omega_g/2\pi)$$

indicates that the fourth harmonics of Ω_1 and Ω_2 are leaving the phonon band. It is precisely at $t\approx 375$ that Y, in Fig. 10(b), stops decreasing and begins to increase.

We also observe in Figs. 10(d) and 10(f) that the velocities of the forward and backward subkinks are slightly different in the untrapped regime. This is due to the fact that the phonons are not radiated away from the kink exactly in the same manner in the backward and forward directions of the moving kink. In this respect we recall that in the phonon-radiation process each subkink emits a part of phonons in the direction of the other subkink. The phonons emitted by the forward subkink (X_1) in the direction of the backward subkink (X_2) quickly arrive within the backward subkink (X_2), and pass through this subkink while the system is still in the untrapped regime, before being radiated away from the DSG kink. On the other hand, the phonons emitted by the backward subkink (X_2) in the direction of the forward subkink (X_1) move in the same direction as the whole kink and therefore those phonons must cover a much larger distance before attaining the forward subkink (X_1). Those phonons begin to pass through the forward subkink (X_1) when the system has already made a transition to the trapped regime. Thus the slight difference observed between the velocities of the two subkinks in the untrapped regime is due to the effects of the phonons which are passing through the subkink (X_2).

B. Kink dynamics for $L_0=5.588, \Re=4\pi/L_0\approx 2.2488$

When the parameter $\Re$ becomes sufficiently small, the subkinks of the DSG kink overlap. The DSG kink should therefore be treated as a single collective entity described by the collective variables X and Y. For instance, in the case that we now consider, that is, $\Re=4\pi/L_0\approx 2.2488$, the quantity $\mathcal{D}=X_2-X_1=2(\Re+Y)/\omega_0$ (that we used previously for evaluating the separation between the subkinks) reduces to only four lattice cells when $Y=0$. Moreover, we observe in Fig. 11, which shows the static profile of a discrete DSG kink

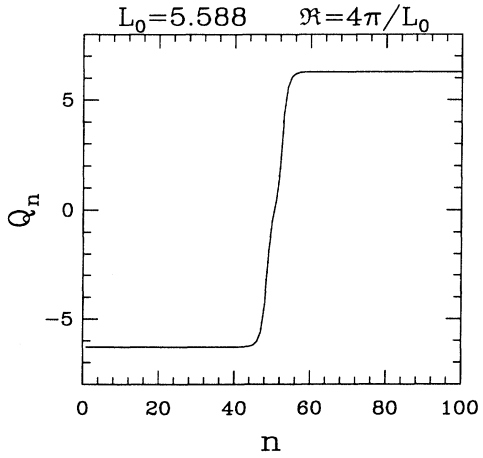

FIG. 11. Profile of the discrete DSG kink centered at $X=50.5$ in a 100 particle chain, for $L_0=5.588$ and $\Re=4\pi/L_0$.

for $\Re=4\pi/L_0$, that the subkinks have actually lost their individual identities.

Before performing the kink dynamics, it is interesting to first examine the shape of the PN potential in the present case, in order to facilitate our understanding of the dynamics later on. In this respect we recall that in the case considered previously, that is, $\Re=26\pi/L_0\approx 14.617$, the subkinks do not overlap and each subkink is embedded in a PN well whose minimum is located midway between two adjacent lattice sites. On the other hand, we observe in Fig. 12(a), which shows one period of the PN potential of the DSG kink for $\Re=4\pi/L_0$, the striking behavior that each period of the PN potential now possesses two wells in each lattice cell, whose minima are located, respectively, at $X=m$ and $X=m+\frac{1}{2}$[$m=0$ in the case of Fig. 12(a)]. Note that this behavior is in marked contrast with the behavior found in most of the discretized field theories [12–14], where each period of the PN potential possesses only a single well. However, such discreteness effects may well be generic features in the sense that they were already mentioned in previous work for some other deformable substrate potentials [15,6].

We must also stress the following point: we have

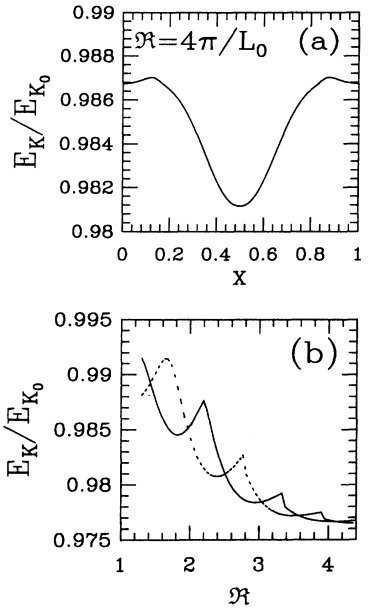

FIG. 12. Plot of the normalized discrete kink's energy for $L_0=5.588$. (a) shows the shape of the PN potential within a lattice cell for $\Re=4\pi/L_0$. (b) shows the kink's energy versus $\Re$ for a kink centered on a particle of the chain, $X=m$ (solid curve), and for a kink centered midway between two adjacent lattice sites, $X=m+\frac{1}{2}$ (dotted curve). Note for (a) that for obtaining the kink energy one needs first to obtain the static kink profile for each X. For performing the relaxation of the kink for $X\neq m, m+1/2$, that is, away from its equilibrium positions, one must let the system relax subject to an external force, otherwise the kink will relax at one of its two equilibrium positions, $X=m$ or $X=m+1/2$.

found that the shape of the PN potential depends strongly on $\Re$, so that there exist in the system some other types of behavior than the one shown in Fig. 12(a). For instance, Fig. 12(b) shows the plot of the normalized energy of the discrete DSG kink, $E_K(X)/E_{K_0}$, versus $\Re$, for $X=m$ (solid curve) and $X=m+\frac{1}{2}$ (dotted curved). $E_{K_0}\equiv M_{0_Y}$ is the continuum kink rest energy given by Eq. (3.15). Figure 12(b) exhibits three types of behavior.

(i) In some parameter regions, $E_K(X=m+\frac{1}{2})<E_K(X=m)$; which corresponds to the same case as the one shown in Fig. 12(a), where the deepest well of the PN potential is located midway between two adjacent lattice sites.

(ii) In some other parameter regions, however, $E_K(X=m+\frac{1}{2})>E_K(X=m)$; which corresponds to a case where the deepest well of the PN potential is located exactly on each lattice site.

(iii) For some values of $\Re$, $E_K(X=m+\frac{1}{2})=E_K(X=m)$; thus implying that the two minima of the PN potential become degenerate.

In the forthcoming discussions we focus on the case (i) and examine the dynamics for $\Re=4\pi/L_0$. For performing the dynamics, we will always consider a kink which is initially at rest in the bottom of the PN well with the smallest depth, that is, a kink centered at

$$X(t=0)=1001\ ,$$

in a 2000 particle chain. The shape of the PN potential in Fig. 12(a) then allows us to foresee that one can obtain three types of regimes for the kink dynamics depending upon the magnitude of the initial velocity of the c.m.

1. *Trapped regime in the well with the smallest depth, for $\Re=4\pi/L_0$*

Figures 13(a) and 13(b), obtained for $\epsilon_X=-0.0004$, $\epsilon_Y=0$ [which corresponds to $\dot{X}(t=0)=-0.014\,38$, $\dot{Y}(t=0)=0$], show that when the initial velocity is sufficiently small but nonzero the kink moves off its equilibrium position (in the well with the smallest depth) and attempts to proceed to the deepest well of the PN potential, but finds that it cannot do so because its kinetic energy is not sufficient for crossing the intervening PN barrier. The kink is therefore definitively trapped in this shallow well during the ensuing motion. Furthermore, we see in Figs. 13(a) and 13(b) that during this motion the amplitudes of oscillation of X and Y remain essentially constant; which indicates that the radiation emitted by the kink is negligible.

2. *Trapped regime in the deepest well of the PN potential, for $\Re=4\pi/L_0$*

When one increases the initial velocity (compared to the case of Fig. 13) one attains a small region of $\dot{X}(t=0)$, given by $0.0005\leq|\epsilon_X|\leq 0.001$, in which the initial kinetic energy becomes just enough to permit the kink to cross the first intervening PN barrier. The kink then moves up to the deepest PN well before undergoing the trapping in this well. Figure 14 shows the results obtained for

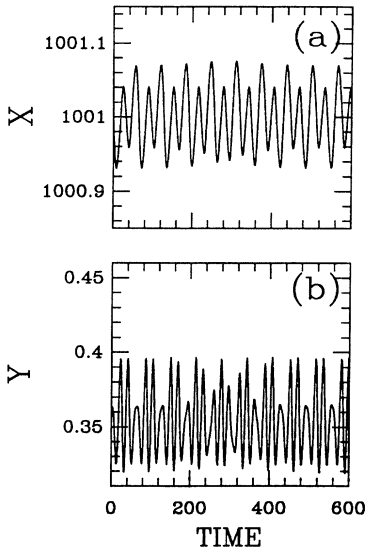

FIG. 13. Kink dynamics for $L_0=5.588$ and $\Re=4\pi/L_0$. (a) $X(t)$; (b) $Y(t)$. The simulation parameter are $\epsilon_X=-0.0004$ and $\epsilon_Y=0, \Delta t=\pi/113.5$, and $N=2000$.

$\epsilon_X=-0.001$, $\epsilon_Y=0$ [$\dot{X}(t=0)=-0.035\,947$, $\dot{Y}(t=0)=0$]. As expected, the amplitudes of oscillation for X and Y, in Figs. 14(a) and 14(b) are much larger than for the case of Fig. 13 (where the kink is trapped in the shallow well). Moreover, the kink now radiates away energy more strongly, as illustrated in Fig. 14(d), which

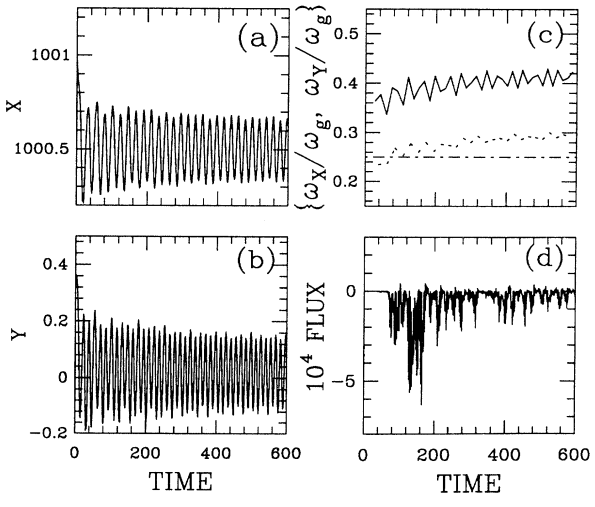

FIG. 14. Kink dynamics for $L_0=5.588$ and $\Re=4\pi/L_0$. (a) $X(t)$; (b) $Y(t)$; (c) $\omega_X(t)/\omega_g$ (dotted curve) and $\omega_Y(t)/\omega_g$ (solid curve); (d) instantaneous Poynting's flux evaluated at the lattice site no. 976. The simulation parameters are $\epsilon_X=-0.001$ and $\epsilon_Y=0, \Delta t=\pi/227$, and $N=2000$. In (c), we have drawn a horizontal dotted line at 0.25 in order to indicate that the fourth harmonic of ω_X resonates with the phonon modes during the motion.

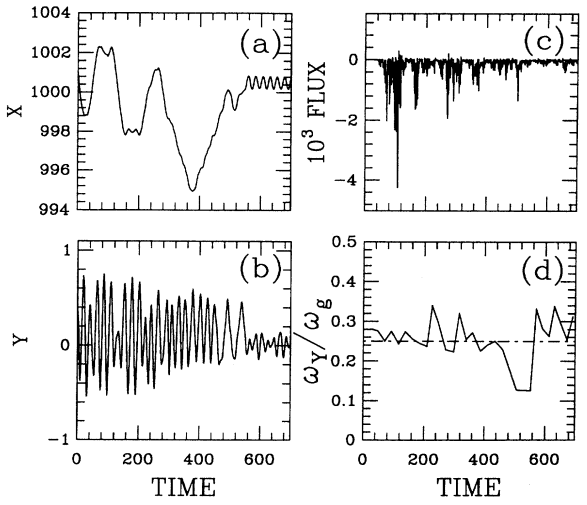

FIG. 15. Kink dynamics for $L_0=5.588$ and $\Re=4\pi/L_0$. (a) $X(t)$; (b) $Y(t)$; (c) instantaneous Poynting's flux evaluated at the lattice site no. 976; (d) $\omega_Y(t)/\omega_g$. The simulation parameters are $\epsilon_X=-0.00525$ and $\epsilon_Y=0, \Delta t=\pi/454$, and $N=2000$. In (d), we have drawn a horizontal dotted line at 0.25 in order to indicate that the fourth harmonic of ω_Y resonates with the phonon modes during the motion.

shows the time evolution of the Poynting's flux of the phonon radiation evaluated 25 lattice sites away from the center of the kink. The discrete definition of the Poynting's flux S is [10]

$$S(n_0,t)=-\left\{\frac{Q_{n_0}(t+\Delta t)-Q_{n_0}(t)}{\Delta t}\right\} \times\{Q_{n_0+1}(t)-Q_{n_0}(t)\} \quad , Q_{n_0}(t)=f_{n_0}+q_{n_0} ,$$

where n_0 designates the lattice site where one evaluates the flux. In the case of Figs. 14(d), $n_0=976$.

Figure 14(c), which shows the time evolution of the frequencies for X and Y, reveals that the fourth harmonic of ω_X enters the phonon band at about $t=70(\omega_X=\omega_g/4)$, which leads to the emission of a burst of phonons from the kink. Then those phonons travel through 25 lattice sites before attaining the site no. 976 (where we evaluate the flux). The peaks which appear in Fig. 14(d), for $t>70$, are due to those phonons passing through the lattice site no. 976.

3. *Untrapped regime for* $\Re=4\pi/L_0$

When the magnitude of the initial velocity begins to become important, the kinetic energy of the kink becomes sufficient to permit the kink to overcome the intervening PN barriers. The kink therefore goes through the untrapped regime in the beginning of its motion. Figures 15(a)–15(d), which show the results obtained for $\epsilon_X=-0.005\,25$, $\epsilon_Y=0$ $[\dot{X}(t=0)=-0.188\,724\,28$, $\dot{Y}(t=0)=0]$, reveal some major differences with respect to the case considered in Fig. 10 (where $\Re$ is relatively large). Indeed, we observe in Fig. 10(a) that the kink travels through 53 lattice cells, *at one go,* before undergoing the transition to the trapped regime. On the other hand, we find in Fig. 15(a) that in the untrapped regime the kink undergoes several *temporary trappings* in some lattice cells, and also some *reflections back* with respect to the direction of the initial velocity, and finally finds itself definitively trapped between the lattice cells no. 1000 and no. 1001, that is, precisely inside its initial PN well.

Moreover, a careful examination of Figs. 15(a) and 15(b) shows that as soon as the dynamics begin the kink travels through the lattice in the negative x direction up the lattice cell no. 999, where the first temporary trapping occurs. Figure 15(b) shows that this temporary trapping occurs precisely as the amplitude of oscillation of Y attains its maximum; which indicates that the temporary trapping occurs precisely when a relatively large packet of energy that was initially stored in the c.m. mode is transferred to the internal mode. Then, after a while, the energy lost by the c.m. mode is at least in part restored while the kink is moving in the positive x direction. The kink therefore begins again to cross the PN wells and travels in the positive x direction up to the lattice cell no. 1002, where the second temporary trapping occurs. This behavior illustrates once more the effects of the energy-exchange process between the c.m. mode and the internal mode on the motion of the discrete DSG kink. A similar behavior was already observed for a deformable double well substrate potential [6]. Thus, when one compares the behavior in Figs. 10(a) and 15(a), it appears that the temporary-trapping phenomenon occurs in the DSG system when the parameter $\Re$ becomes sufficiently small; which corresponds to the case where X and Y interact strongly.

Furthermore, we see in Fig. 15(c) that the Poynting's flux exhibits several peaks, and Fig. 15(d) shows that during the untrapped regime the frequency of oscillation of Y oscillates about $\omega_g/4$. Those oscillations in the time evolution of ω_Y, which are due to the interactions between X and Y, indicate that the fourth harmonic of ω_Y often enters the phonon band but goes out after a while. Each time that the fourth harmonic of ω_Y enters the phonon band the kink emits a burst of phonons; hence the peaks observed in Fig. 15(c).

In the following section we conclude the present work.

V. CONCLUSION

Collective variable theories have been successful in treating internal modes such as those that appear in the DSG equation and other Klein-Gordon equations. They have also been effective qualitatively and quantitatively in describing discreteness effects such as the PN potential and the radiation by untrapped kinks at the frequency $\Omega=2\pi\dot{X}$ and trapped kinks at the harmonics of the PN frequency. In the case of internal modes the radiation occurs at harmonics of the internal mode oscillation frequency. In this paper we have found the separate discrete and internal mode effects for the DSG kink. Here we summarize only the qualitatively different phe-

nomena that result from the occurrence of both discreteness and internal modes.

The dimensionless parameter that measures discreteness in the DSG system is $(2\pi/L_0)$. When this parameter is small $(2\pi/L_0)\ll 1$, or equivalently $L_0 \gg 2\pi$, we have the continuum limit and when the parameter is greater than 1 we have a very discrete system. The second important dimensionless parameter is the ratio of the distance $\mathcal{D}_0$ between the subkinks, Eq. (2.11), to the size of the subkink L_0, i.e., $\mathcal{D}_0/L_0=\Re/\pi$. When $\Re \gg \pi$, Fig. 6, the subkinks are far apart and we can think of them roughly as SG kinks although the distance between them is still determined by $\Re$. In the case $\Re < \pi$, Fig. 11, the subkinks no longer have separate identities. In the large-kink limit $(\Re \gg \pi)$ we find when the trapped kink is excited initially such that $R(t=0)=\Re$, that is, $Y(t)=0$, Fig. 7(c), that, as a consequence of asymmetry in the forward and backward directions of radiation from a moving kink at the harmonics of ω_X, the distance between the subkinks is changed and thus the internal mode is excited. Thus in the DSG system the effect of phonon radiation on the different subkinks is responsible for the excitation of the internal mode. In the untrapped large-kink case, when the kink is set in motion with the internal mode unexcited initially, we again find that as a result of asymmetric phonon radiation the internal mode is excited. We also find that the two subkinks travel at slightly different velocities due to the asymmetry of the radiation of phonons in the forward and backward directions. When the untrapped kink eventually becomes trapped the R mode oscillates not about $\Re$ but about a value smaller than $\Re$. We also observe the usual result in the untrapped case that as the kink radiates its velocity decreases and so does the Doppler frequency $2\pi\dot{X}$, and its harmonics which were initially inside the phonon band pass out through the bottom of the band and are no longer able to radiate. The condition for the nth harmonic to become nonradiating is $n(2\pi\dot{X})=\omega_g$.

For the small kink, there is a richer spectra of behavior than there is for the large-kink case. Most of the richness comes from the fact [Fig. 12(a)], that there are two minima per unit cell located at $X=m$ and $X=m+\frac{1}{2}$. There are three cases where $E_K(X=m+\frac{1}{2})$ is greater than, less than, or equal to $E_K(X=m)$. It is sufficient to discuss a single case $E_K(X=m+\frac{1}{2})>E_K(X=m)$. When a kink starts out in the lesser depth well with a kinetic energy less than that required to leave the shallower well it is trapped and since the frequency scales with the depth of the well the frequency of oscillation is small compared with the band edge frequency. Consequently, the radiation is weak because such a high harmonic of the frequency is required in order to be resonant with the phonon band.

In the untrapped small-kink case we find the greatest qualitative difference from previously treated cases. We find that the DSG kink undergoes several temporary trappings before finally radiating sufficient energy to be trapped. The reason for the temporary trapping is that energy from the c.m. X is converted into internal mode energy and the kink becomes temporarily trapped due to the loss of c.m. energy. However, the internal mode transfers an appreciable part of its energy back to the c.m. which then causes the DSG kink to become untrapped. All during this process the kink is radiating energy in both the $X(t)$ and $R(t)=Y(t)+\Re$ modes and so eventually the kink becomes permanently trapped. We see in Figs. 14(c) and 15(d), and in the plots of the Poynting's flux, the bursts of radiation when the harmonics of ω_X or ω_Y enters the phonon band as well as the intervals of decreased radiation when modes exit the phonon band.

In conclusion, we have seen how the lowest-order approximation to the exact CV theory, which consists of the ordinary differential equations for the collective variables $X(t)$ and $R(t)$ coupled to the linearized equations of motion for the phonons, can explain qualitatively (and semiquantitatively) the behavior of the discrete DSG system. It would be extremely difficult to extract comparable information from $\phi(n,t)$ by any perturbation theory that did not introduce collective variables. For example, we can explain the phonon radiation by taking the lowest-order perturbation approximation of our exact CV equations. Another example, the exchange of energy between $X(t)$ and $R(t)$, would be extremely difficult to describe from $\phi(n,t)$ without collective variables. We conclude with the observation that other discrete nonlinear Klein-Gordon systems with internal modes, such as ϕ^4, can be treated by the same approach that we used for the DSG equation in this paper.

ACKNOWLEDGMENT

One of us (C.R.W.) would like to thank M. Perez for useful conversations.

[1] C. Willis, M. El-Batanouny, S. Burdick, and R. Boesch, Phys. Rev. B **35**, 3496 (1987).
[2] D. K. Campbell, M. Peyrard, and P. Sodano, Physica D **19**, 165 (1986).
[3] D. K. Campbell, J. F. Schonfeld, and C. A. Wingate, Physica D **1**, (1983).
[4] R. Ravelo, M. El-Batanouny, C. R. Willis, and P. Sodano, Phys. Rev. B **38**, 4817 (1988).
[5] R. Boesch, P. Stancioff, and C. R. Willis, Phys. Rev. B **38**, 6713 (1988).
[6] P. Tchofo Dinda and C. R. Willis, Physica D **70**, 217 (1993).
[7] S. Flach and C. R. Willis, Phys. Rev. E **47**, 4447 (1993).
[8] R. Boesch and C. R. Willis, Phys. Rev. B **39**, 361 (1989).
[9] C. Willis, M. El-Batanouny, and P. Stancioff, Phys. Rev. B **33**, 1904 (1986).
[10] R. Boesch, C. R. Willis, and M. El-Batanouny, Phys. Rev. B **40**, 2284 (1989).

[11] M. Peyrard and M. D. Kruskal, Physica D **14**, 88 (1984).
[12] P. Tchofo Dinda, R. Boesch, E. Coquet, and C. R. Willis, Phys. Rev. B **46**, 3311 (1992).
[13] J. Andrew Combs and Sidney Yip, Phys. Rev. B **28**, 6873 (1983).
[14] C. R. Willis and R. Boesch, Phys. Rev. B **41**, 4570 (1990).
[15] M. Peyrard and M. Remoissenet, Phys. Rev. B **26**, 2886 (1982).